ARTICLE **Communicated by Christian Bick**

Pulse Shape and Voltage-Dependent Synchronization in Spiking Neuron Networks

Bastian Pietras
bastian.pietras@upf.edu
Department of Information and Communication Technologies, Universitat Pompeu Fabra, 08018, Barcelona, Spain

Pulse-coupled spiking neural networks are a powerful tool to gain mechanistic insights into how neurons self-organize to produce coherent collective behavior. These networks use simple spiking neuron models, such as the θ-neuron or the quadratic integrate-and-fire (QIF) neuron, that replicate the essential features of real neural dynamics. Interactions between neurons are modeled with infinitely narrow pulses, or spikes, rather than the more complex dynamics of real synapses. To make these networks biologically more plausible, it has been proposed that they must also account for the finite width of the pulses, which can have a significant impact on the network dynamics. However, the derivation and interpretation of these pulses are contradictory, and the impact of the pulse shape on the network dynamics is largely unexplored. Here, I take a comprehensive approach to pulse coupling in networks of QIF and θ-neurons. I argue that narrow pulses activate voltage-dependent synaptic conductances and show how to implement them in QIF neurons such that their effect can last through the phase after the spike. Using an exact low-dimensional description for networks of globally coupled spiking neurons, I prove for instantaneous interactions that collective oscillations emerge due to an effective coupling through the mean voltage. I analyze the impact of the pulse shape by means of a family of smooth pulse functions with arbitrary finite width and symmetric or asymmetric shapes. For symmetric pulses, the resulting voltage coupling is not very effective in synchronizing neurons, but pulses that are slightly skewed to the phase after the spike readily generate collective oscillations. The results unveil a voltage-dependent spike synchronization mechanism at the heart of emergent collective behavior, which is facilitated by pulses of finite width and complementary to traditional synaptic transmission in spiking neuron networks.

1 Introduction

Self-organization in large neural networks crucially relies on rapidity, and precision, in short, highly effective neuronal communication. Brisk synaptic

Neural Computation **36, 1476–1540** (2024)
https://doi.org/10.1162/neco_a_01680

interactions allow for emergent collective behavior and can orchestrate neural synchronization, which is believed to be fundamental to cognitive functions and consciousness. A key player in the synaptic transmission process is the spike—that is, the action potential of a neuron. As a central information unit of the brain it has risen to fame and fortune (Wilson, 1999; Gerstner & Kistler, 2002; Humphries, 2021). Spikes are believed to be critical for information processing and coding, and more so as the basis of communication among neurons. Once the membrane potential of a neuron exceeds some threshold, the soma quickly depolarizes and the neuron spikes. Straight off, a fast electrical impulse travels along the neuron's axon to the presynaptic knobs, where it triggers various biochemical processes to release neurotransmitters and eventually induce a postsynaptic current in the connected cell (Destexhe et al., 1994; Sabatini & Regehr, 1999; Lavi et al., 2015; Wang & Dudko, 2021).

In developing a mechanistic understanding of the collective behavior of large neural networks, incorporating a high degree of biological detail is challenging. For computational and mathematical convenience, pulse-coupled spiking neuron networks have been proposed. This approach proves instrumental in comprehending the information processing capabilities of neurons and enables efficient simulation of neural networks. In these pulse-coupled spiking neuron networks, synaptic interactions are typically modeled using δ-spikes, defined here as infinitely narrow Dirac δ-pulses emitted by presynaptic neurons at their spike times. The term *pulse* specifically refers to the chemical synaptic transmission process, whereas *spike* signifies the firing of an action potential. Biologically intricate synaptic transmission is reduced to the causal effect of a Dirac δ-pulse—which in fact resembles a spike—initiating a response in the connected postsynaptic neuron. A similar reductionist approach is integral to spiking neuron models, focusing on subthreshold membrane properties while excluding mechanisms responsible for generating action potentials (i.e., voltage-dependent sodium and potassium channels). The firing of an action potential, or a neuron's *spike*, occurs instantaneously upon reaching a specific membrane potential threshold, yet its actual dynamics is left unspecified. The neuron's spike induces a presynaptic pulse that will be perceived by any connected postsynaptic neuron. While often simplified to a δ-spike, this spike-pulse interaction at the presynaptic site can assume various forms and shape the collective dynamics. This is a central theme of this work.

On an individual level, the assumption of instantaneous spikes is most successfully caricatured in integrate-and-fire neuron models (Burkitt, 2006). But also in biophysically realistic Hodgkin-Huxley-like conductance-based neuron models, the spike generation can be rapid compared to relatively slow subthreshold integration. The separation of timescales becomes extreme if neurons are class 1 excitable and near the onset of firing. Ermentrout and Kopell (1986) proved that any such class 1 excitable neuron can be transformed into a canonical, one-dimensional phase model—the θ-neuron

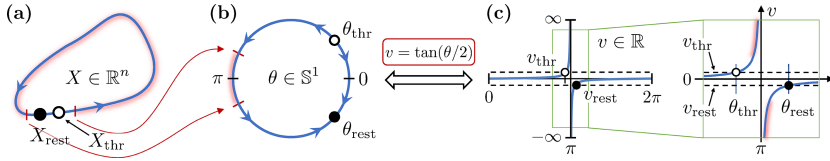

Figure 1: Reduction from (a) a high-dimensional, conductance-based neuron model close to a SNIC bifurcation to (b) the one-dimensional canonical θ-neuron model with $\eta < 0$. The trajectory describing the action potential along the limit cycle is shaded in red and compressed around π in the θ-neuron. Via the transform $v = \tan(\theta/2)$, the θ-neuron is equivalent to (c) the QIF neuron when reset and peak values are taken at infinity.

(see Figure 1). It is one of the simplest spiking neuron models and closely related to the quadratic integrate-and-fire (QIF) neuron (Ermentrout, 1996).

In network models of these spiking neurons, the default description of synaptic interactions is with δ-spikes, but a growing number of studies have proposed synaptic transmission via pulses of finite width. This raises the question of how pulses of finite width should be interpreted. They may represent the release of neurotransmitters at the presynaptic site, the conversion of neurotransmitter signals into postsynaptic currents at the postsynaptic site, or a combination of both. Despite widespread use, the nature of these pulses remains largely unclear. Meanwhile, the shape of the pulse is critical for neuronal synchronization and can either facilitate or impede collective oscillations. Currently, however, there is no definitive understanding how the pulse shape affects collective dynamics.

In this article, I revisit the use of pulse coupling in networks of QIF and θ-neurons to provide, first, a clear biological interpretation for pulses of finite width and, second, a comprehensive view on the impact of the pulse shape on the collective dynamics of globally coupled spiking neurons. A better understanding of these fundamental aspects of synaptic transmission will greatly contribute to our understanding of neural network behavior.

1.1 The Pulse Problems of θ- and QIF Neurons. QIF and θ-neurons are two paradigmatic spiking neuron models. Each is a canonical model for biologically detailed conductance-based neurons and can be derived from realistic, high-dimensional neuronal dynamics (Hoppensteadt & Izhikevich, 1997). On the individual level, QIF and θ-neurons are closely related; they become equivalent if threshold and reset values of the QIF neuron are taken at infinity (see Figure 1). In network models, however, pulsatile synaptic interactions between QIF neurons are often modeled differently from those between θ-neurons. This dichotomy stems in part from the difficulty of deriving canonical network models from networks of synaptically coupled conductance-based neurons. Such a network reduction is more challenging,

if at all possible, than a single neuron reduction (Hoppensteadt & Izhikevich, 1997; Pietras & Daffertshofer, 2019). Therefore, pulse-coupled spiking neural networks often lack mathematical rigor, especially when refraining from δ-spike interactions (but see section 2.2).

Given the opposing approaches to pulse coupling in networks of QIF or of θ-neurons, it is inevitable to question the biological plausibility of pulses of finite width. Shall those pulses replicate the biochemical processes at the presynaptic site (converting the presynaptic action potential into the release of neurotransmitters), at the postsynaptic site (converting the neurotransmitter signal into a postsynaptic current), or at both sites? Moreover, and to retain the computational advantages of spiking networks, pulses are usually defined as functions of the state variable of the presynaptic neuron. This can be limiting because chemical synaptic transmission is a dynamic process that, in fact, involves both presynaptic and postsynaptic neurons. It would thus be consistent to restrict the interpretation of those pulses to the presynaptic site of a synapse, where the pulse reflects the conversion from an action potential into the release of neurotransmitter. The state variables of the QIF and of the θ-neuron, however, do not describe realistic voltage traces in the course of an action potential—in contrast to conductance-based neuron models (from which they may have been reduced). It is therefore not clear if the pulse function can actually relate the state variables to voltage-dependent mechanisms that eventually trigger neurotransmitter release. In sections 2.2 and 2.3, I revisit pulsatile interactions between θ-neurons and between QIF neurons, and propose biologically plausible interpretations for pulses of finite width with symmetric and asymmetric shapes.

Next to a clear and biologically plausible interpretation, the other "pulse problem" is the largely unexplored effect of the pulse shape on the collective dynamics of pulse-coupled QIF or θ-neurons. Pulses of finite width have frequently been used in the literature to describe synaptic interactions especially between θ-neurons, but also between QIF neurons. Most of the time, the pulses are assumed to be symmetric about the neuron's spike time without varying the shape much. The mechanisms by which the pulse shape can affect the network dynamics, promote synchrony, and induce collective oscillations even for instantaneous coupling, remain largely unknown.

A few insights, though, can be borrowed from the vast results on coupled phase oscillators—the phase representation of the θ-model invites one to invoke phase oscillator theory; nonetheless, direct analogies should be regarded with care (see section 5.1). Traditionally, the Winfree model (Winfree, 1967, 1980) has paved the way to study synchronization of periodically firing neurons. It pinpoints a pulse-response coupling, where the pulse can be shown to result from the interplay between presynaptic action potential and a synaptic activation function ("voltage-dependent conductance"; Ermentrout & Kopell, 1990). Furthermore, the Winfree model has allowed for exploring the effect of the response and pulse functions on synchronization properties of the network (Ariaratnam & Strogatz, 2001; Pazó &

Montbrió, 2014; Gallego et al., 2017). Similarly, coupled active rotators (Shinomoto & Kuramoto, 1986; Kuramoto et al., 1987) served as a basis to study how the width of (symmetric) pulses affects collective dynamics (O'Keeffe & Strogatz, 2016). In line with the results on the Winfree model, broad pulses were reported to entail collective dynamics that can be different from those generated by narrow pulses (Pazó & Montbrió, 2014; Gallego et al., 2017; O'Keeffe & Strogatz, 2016); it remains unclear, however, how these results carry over to networks of θ-neurons. A crucial tool for distilling the effect of the pulse shape on the collective dynamics of Winfree oscillators and active rotators has been an exact dimensionality reduction first proposed by Ott and Antonsen (2008). Although immensely powerful, the Ott-Antonsen ansatz requires the pulse function to be analytically tractable, which may come at the cost of biological realism. The introduction of the Ott-Antonsen ansatz in networks of θ-neurons (Luke et al., 2013) has inspired a plethora of θ-neuron network studies using symmetric and broad pulses ever since (So et al., 2014; Luke et al., 2014; Laing, 2014, 2015, 2016a, 2016b; Roulet & Mindlin, 2016; Laing, 2017; Chandra et al., 2017; Laing, 2018a, 2018b; Aguiar et al., 2019; Lin et al., 2020; Laing & Bläsche, 2020; Laing & Omel'chenko, 2020; Means et al., 2020; Bläsche et al., 2020; Bick et al., 2020; Jüttner et al., 2021; Omel'chenko & Laing, 2022; Bîrdac et al., 2022). Despite the prevailing uncertainty of their biological interpretation, these pulses now seem well established in the community. Still, a comprehensive picture of how their width influences collective dynamics is missing. On top of it, they are not versatile enough either to study the effect of pulse asymmetry. In a nutshell, a systematic investigation how the pulse shape—symmetric or asymmetric—affects the collective dynamics of θ- or QIF neurons has remained elusive.

1.2 Synopsis and Outline. I strive for resolving the pulse problems of θ- and QIF neurons, first, by providing a biological interpretation for pulses of finite width and second, by analyzing the impact of the pulse shape on the collective dynamics.

As to the biophysical interpretation of pulses of finite width, I present two alternative views in section 2 that are equally valid but depend on the particular modeling assumptions. The connection between θ- and QIF neurons confounds a clear separation of these alternative interpretations, as one can easily transform one model into the other. Yet there is a subtle difference between the two spiking neuron models (see section 2.1). In the context of weakly coupled class 1 excitable neurons close to the onset of firing, pulses in the canonical network model of θ-neurons can describe instantaneous synaptic transmission at both the pre- and postsynaptic sites; these pulses can have arbitrary shapes as long as they are sufficiently narrow (see section 2.2). When one regards QIF neurons as "the simplest model of a spiking neuron" (Izhikevich, 2007) irrespective of the foregoing network setting, I show in section 2.3 how to introduce voltage-dependent pulses

$p(v)$ that replicate the transmission process of conductance-based neurons exclusively at the presynaptic site. Crucially, I propose a modification of the synaptic activation function p to account for the artificial shape of the QIF's action potential.

The correspondence between the QIF and the θ-model allows one to use the two pulse interpretations in θ- and QIF networks interchangeably; nonetheless, I advise caution not to mix up the respective underlying assumptions. Toward analytic tractability, I capitalize on the QIF-θ-correspondence in section 2.4 and approximate the voltage-dependent pulses $p(v)$ by pulses $p_{r,\varphi,\psi}(\theta)$ formulated in terms of the θ-phase via $\theta = 2\arctan(v)$. The pulse parameters r, φ, ψ allow for interpolating between discontinuous δ-spikes and continuous pulses of finite width with symmetric or asymmetric shapes, enabling a systematic study how the pulse shape affects the collective dynamics of the network.

Conveniently, the family of smooth pulse functions $p_{r,\varphi,\psi}(\theta)$ is admissible to an exact reduction of globally coupled spiking neurons in the thermodynamic limit (Pietras et al., 2023), Here, I build on recent advances in coupled oscillator theory (Ott & Antonsen, 2008; Cestnik & Pikovsky, 2022a, 2022b), which allows for a comprehensive analysis of the collective dynamics thanks to an exact mean-field description in terms of the firing rate R and the mean voltage V (section 3). Taking the population average yields an expression of the mean pulse activity $P_{r,\varphi,\psi} = \langle p_{r,\varphi,\psi} \rangle$ that is fully determined by R and V. For instantaneous synaptic transmission, the exact mean-field dynamics converges toward an invariant two-dimensional manifold (Pietras et al., 2023), on which the ordinary differential equations for the firing rate and voltage (RV dynamics) are closed in R and V (Montbrió et al., 2015). Section 4 is devoted to the mathematical analysis of the two-dimensional RV dynamics. I analyze how the different pulse parameters—width r, asymmetry φ, and shift ψ—affect the region of collective oscillations and prove that collective oscillations emerge due to an effective coupling through the mean voltage V (see section 4.1). This voltage-dependence readily arises for global pulse coupling as $P_{r,\varphi,\psi} = P_{r,\varphi,\psi}(R, V)$ explicitly depends on V, except for the limit of δ-spikes, $(r, \varphi, \psi) \to (1, 0, \pi)$. In other words, pulse-coupling generally facilitates collective oscillations through an effective voltage coupling, but if neurons interact via δ-spikes, the recurrent input no longer depends on the mean voltage and collective oscillations become impossible. Moreover, the pulse shape determines the effectiveness of the pulse-mediated voltage coupling and thus plays a crucial role for the emergence of collective oscillations. For symmetric pulses, collective oscillations are confined to a small parameter region and require unrealistically strong inhibition the narrower the pulse (see section 4.2). Additionally, broad symmetric pulses have a nongeneric effect on the collective dynamics that is not present in narrow pulses (see also Pazó & Montbrió, 2014; O'Keeffe & Strogatz, 2016; Gallego et al., 2017). In contrast to symmetric pulses, narrow pulses that are slightly skewed to the phase after

the spike readily generate collective oscillations in networks of inhibitory neurons (see section 4.3), whereas pulses that are slightly skewed to the phase before the actual spike generate collective oscillations among excitatory neurons (see section 4.4). Together, the results shed new light on the voltage-dependent spike synchronization mechanism that is typically not captured in traditional mean-field, or firing rate, models (Wilson & Cowan, 1972), but crucially underlies collective oscillations in neural networks.

In the discussion in section 5, I first review previous approaches to pulse coupling in networks of spiking neurons, which may have led to misconceptions about the interpretation and the effect of pulses of finite width in networks of θ- and QIF neurons (section 5.1). I then revisit the three pulse parameters in more detail and draw connections to delayed synaptic interactions and electrical coupling via gap junctions (see section 5.2). Finally, I return to the question of whether instantaneous pulses of finite width can replace more complex synaptic transmission in spiking neuron networks including synaptic kinetics and conductance-based synapses—I argue in the negative (section 5.3). Conclusions, final remarks, and an outlook are provided in section 6. Mathematical details are in online appendixes A to H.

2 Pulses in Spiking Neuron Networks

2.1 Two Canonical Spiking Neuron Models. I focus on (1) the "theta"-neuron as the canonical model for class 1 excitable[1] neurons close to saddle-node bifurcation on an invariant circle (SNIC bifurcation) and on (2) the quadratic integrate-and-fire (QIF) neuron as the canonical model for a biologically detailed conductance-based neuron close to a saddle-node bifurcation (Hoppensteadt & Izhikevich, 1997). "Canonical" means that in the first case, any class 1 excitable neuron close to a SNIC bifurcation can be reduced to a one-dimensional neuron with a phase variable θ, whose dynamics is governed by

$$\dot{\theta} = \frac{d}{dt}\theta(t) = (1 - \cos\theta) + (1 + \cos\theta)\eta \tag{2.1}$$

with excitability parameter η. Despite its formulation in terms of the phase variable θ, equation 2.1 does not result from phase reduction (see also section 5.1). Instead, it is the Ermentrout-Kopell canonical model (Ermentrout & Kopell, 1986; Ermentrout, 1996; Gutkin & Ermentrout, 1998) for a SNIC bifurcation, which occurs when $\eta = 0$. For $\eta < 0$, the neuron is in an excitable regime as the dynamics (see equation 2.1) exhibits a pair of stable and

[1] Class 1 (or I) excitable neurons are also known as type I membranes whose neuronal dynamics exhibit type I excitability.

unstable equilibria. The stable equilibrium represents the neuron's resting state. The unstable equilibrium represents a threshold: when an external input drives the neuron across this threshold, θ will move around the circle in the course of the neuron's action potential and approaches the resting state from below. The neuron is said to fire a spike when θ crosses π. For $\eta > 0$, the two equilibria have disappeared in a saddle-node bifurcation, leaving a limit cycle, and the neuron is in a tonically (periodically) spiking regime. The reduction from a general conductance-based class 1 excitable neuron close to a SNIC bifurcation to the θ-neuron, equation 2.1, is sketched in Figure 1 for $\eta < 0$: close to the saddle-node bifurcation, a small neighborhood of the resting potential is blown up, and the trajectory describing the neuron's action potential along the limit cycle is compressed to an open set around π (shaded in red).

The QIF neuron is characterized by a voltage variable v that follows the subthreshold dynamics,

$$\dot{v} = \frac{d}{dt}v(t) = v^2 + \eta, \tag{2.2}$$

with a fire-and-reset rule: when v exceeds a peak value v_p, the voltage is reset to a reset potential v_r and the neuron is said to elicit a spike. The parameter η plays a similar role as in the θ-neuron, equation 2.1. For $\eta < 0$, there is a pair of stable and unstable equilibria and the QIF neuron will settle into its resting potential at $v = -\sqrt{-\eta}$. For $\eta > 0$ the two equilibria disappear in a saddle-node bifurcation, and the voltage of the QIF neuron will diverge; due to the fire-and-reset mechanism, the neuron then enters into a periodically firing regime.

If peak and reset potentials are taken at infinity, $v_p = -v_r = \infty$, the QIF neuron becomes equivalent to the θ-neuron via the variable transform $v = \tan(\theta/2)$ (see Ermentrout, 1996, and Figure 1). Independent from the equivalence with the θ-model, however, the QIF model has its own right to exist. For example, the QIF dynamics can be obtained from conductance-based neuron models with a parabolic-like voltage nullcline, which is a general feature of Hodgkin-Huxley-like neurons with positive feedback (so-called amplifying) ionic currents, through a quadratization procedure (Rotstein, 2015; Turnquist & Rotstein, 2018). Moreover, the subthreshold QIF dynamics, equation 2.2, is the topological normal form of a saddle-node (fold) bifurcation (Kuznetsov, 1998); the QIF model thus describes any neuronal model close to a saddle-node bifurcation (Hansel & Mato, 2001, 2003). Equipped with finite threshold and reset values, the QIF model is also the simplest spiking neuron model with a spike generation mechanism (i.e., a regenerative upstroke of the membrane potential), with a soft (dynamic) threshold and a spike latency (Izhikevich, 2007). The approximation with infinite threshold and reset values (as considered throughout this work) then allows for valuable insights into the collective dynamics of QIF

neurons as typical class 1 excitable systems, though not necessarily claiming an explicit biophysical interpretation of the underlying neuronal dynamics.

Despite the close interconnection between θ- and QIF neurons, the two canonical spiking neuron models have subtle differences even when the QIF neuron is equipped with finite threshold and reset values. These differences become clear when considering networks of them and when introducing pulse coupling that is different from the commonly employed δ-spikes.

2.2 Pulses in the Canonical Model of Weakly Connected Class 1 Excitable Neurons. Pulse-coupled neural networks are celebrated for their utility and practicability yet are often met with skepticism and dismissed as mere toy models. Nevertheless, a handful of broadly applicable conditions have been distilled to reduce a large class of realistic conductance-based neural network models to a canonical model of pulse-coupled θ-neurons, exhibiting qualitatively identical dynamical properties. Izhikevich (1999) proposed a formal derivation from weakly connected networks of biologically plausible and biophysically detailed class 1 excitable neurons. This derivation yielded θ-neurons coupled through δ-spikes. However, synaptic interactions in the canonical model of pulse-coupled θ-neurons occur not through (discontinuous) δ-spikes but via (smooth) localized pulses of finite width—a distinction I rigorously establish below. These narrow pulses capture the swift impact of a presynaptic action potential, eliciting a postsynaptic response in the connected neuron. Such dynamics result directly from theorem 1 (referenced below), contingent on satisfying the following general conditions (Izhikevich, 1999):

1. Neurons are class 1 excitable; that is, action potentials can be generated with arbitrarily low frequency, depending on the strength of the applied current.
2. Neurons are weakly connected; the amplitudes of postsynaptic potentials (PSP) are much smaller than the amplitude of an action potential or than the mean excitatory PSP size necessary to discharge a quiescent neuron.
3. Synaptic transmission has an intermediate rate, which is slower than the duration of an action potential but faster than the interspike period.
4. Synaptic connections between neurons are of a conventional type, that is, axo-dendritic or axo-somatic.
5. Synaptic transmission is negligible when presynaptic neurons are at rest; spontaneous release of neurotransmitters does not affect significantly spiking of postsynaptic neurons.

These assumptions are generically met by a large class of neural networks, as extensively discussed by Izhikevich (1999) regarding their biological plausibility. In brief, assumption 1 reflects the general belief that the majority of mammalian neurons are actually class 1 excitable (Izhikevich, 1999;

Pfeiffer et al., 2023); assumption 2 reflects the in vitro observation that amplitudes of postsynaptic potentials (PSPs) are much smaller than the mean excitatory PSP necessary to discharge a quiescent cell, and tiny compared to the amplitude of an action potential (Hoppensteadt & Izhikevich, 1997); finally, assumptions 3 to 5 reflect the idea that conventional synaptic transmission occurs from one pre- to one postsynaptic neuron triggered by, and lasting slightly but not much longer than, the presynaptic action potential.

Assumption 1 ensures that an individual conductance-based neuron is close to a SNIC bifurcation, enabling its reduction to the canonical θ-neuron (Ermentrout & Kopell, 1986; Ermentrout, 1996). When embedded in a network and interacting with each other, assumptions 2 to 5 become necessary for the reduction of these neurons to a canonical network model of θ-neurons. Network reduction, however, is significantly more intricate than reducing a single neuron due to the interdependence introduced by coupling terms (Pietras & Daffertshofer, 2019; Hoppensteadt & Izhikevich, 1997). Any transformation simplifying the dynamics of one neuron immediately influences the dynamics of others; therefore, the reduction of a neural network must occur for all neurons simultaneously. I pursue this network reduction in appendix A, where I prove that the canonical network model for weakly coupled class 1 excitable conductance-based neurons is given by pulse-coupled θ-neurons with smooth pulses of short but finite width, as follows:

Theorem 1. *Consider an arbitrary weakly connected neural network of the form*

$$\dot{X}_j = F_j(X_j, \lambda) + \varepsilon G_j(X_1, \ldots, X_N; \lambda, \varepsilon) \tag{2.3}$$

satisfying that each (uncoupled) equation $\dot{X}_j = F_j(X_j, \lambda)$ undergoes a SNIC bifurcation for some $\lambda = \lambda_0$, that each function G_j has the pair-wise connected form

$$G_j(X_1, \ldots, X_N; \lambda_0, 0) = \sum_{k=1}^{N} G_{jk}(X_j, X_k),$$

and each $G_{jk}(X_j, X_k) = 0$ for X_k from some open neighborhood of the saddle-node bifurcation point. Then, there is $\varepsilon_0 > 0$ such that for all $\varepsilon < \varepsilon_0$ and all $\lambda = \lambda_0 + \mathcal{O}(\varepsilon^2)$, there is a piece-wise continuous transformation that maps solutions of equation 2.3 to those of a canonical network model of pulse-coupled θ-neurons, which can be approximated by

$$\theta_j' = (1 - \cos\theta_j) + (1 + \cos\theta_j)\left[\eta_j + \sum_{k=1}^{N} p_{jk}(\theta_k)\right] \tag{2.4}$$

with constants $\eta_j \in \mathbb{R}$. The functions $p_{jk}(\theta_k)$ describe smoothed δ-pulses of strength $s_{jk} = \mathcal{O}(\|G_{jk}\|)$, where $\|.\|$ denotes the supremum norm; that is, the pulse

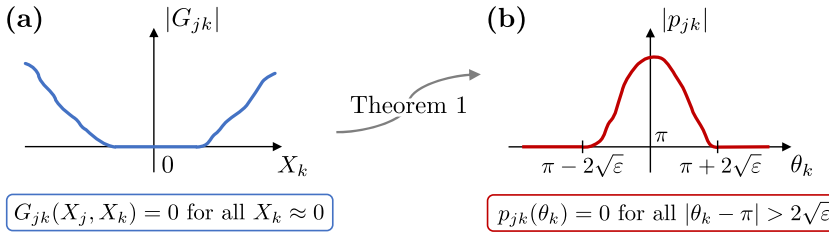

Figure 2: (a) The coupling function G_{jk} of the conductance-based neuron model 2.3 with state variables $X_j \in \mathbb{R}^n$ satisfying assumption 5 has a "dead zone" (Ashwin et al., 2021) around the resting potential $|X_k| = 0$ of postsynaptic neuron k. (b) The smooth pulse function p_{jk} in the pulse-coupled network (see equation 2.4) of θ-neurons is nonzero around the spike time $\theta_k = \pi$ of neuron k and can be derived from weakly coupled class 1 excitable neurons via theorem 1. See also appendix A.

strength is proportional to the amplitude of the coupling in equation 2.3. The duration of every pulse in equation 2.4 is short as $p_{jk}(\theta_k) = 0$ if $|\theta_k - \pi| > 2\sqrt{\varepsilon}$ for all $j, k = 1, \ldots, N$ (see Figure 2).

For the proof of the theorem including all mathematical details, see appendix A.

In the canonical pulse-coupled network equation 2.4, individual θ-neurons are solely characterized by the parameter η_j, whereas the uncoupled dynamics of the underlying neuronal model, equation 2.3, are given by the function F_j describing, for example, a conductance-based Hodgkin-Huxley-like neuron. Interactions between two synaptically connected neurons k and j arise according to assumption 5 only when the presynaptic neuron, say neuron k, is firing a spike. The event of such an action potential lasts $4\sqrt{\varepsilon}$ units of slow time—when θ_k crosses a $2\sqrt{\varepsilon}$-neighborhood of π. As assumption 2 requires that $\varepsilon \ll 1$ is small, it seems reasonable to approximate an emitted pulse by the Dirac δ-function as $p_{jk}(\theta_k) \approx s_{jk}\delta(\theta_k - \pi)$ (see proposition 8.12 in Hoppensteadt & Izhikevich, 1997). In general, however, the pulses $p_{jk}(\theta_k)$ are smooth and of finite width, which can have important consequences for the collective network dynamics depending on the shape of the pulse (see section 4). While an exact reduction of pulse functions p_{jk} from weakly coupled, class 1 excitable, conductance-based neurons is beyond the scope of this work due to technical difficulties detailed in appendix A, exploring the impact of general pulse shapes on the collective dynamics is a valuable pursuit. The θ-neuron network exhibits rich collective behavior already with narrow pulse coupling. For a more comprehensive understanding, I study pulse-coupled networks of θ-neurons with various pulse shapes in section 4, where I consider pulses also beyond

the limits imposed by theorem 1, and discuss their biological interpretation in section 5.3.

Remark 1. The shape of the pulses $p_{jk}(\theta_k)$ in equation 2.4 depends nonlinearly on the shape of the presynaptic action potential (governed by F_j) in interplay with the coupling function G_{jk}. For example, a pulse p_{jk} may describe a conductance-based synapse in the underlying high-dimensional model, equation 2.3, of the form

$$G_{jk}(X_j, X_k) = -g_{\text{syn}}(X_k, t)\big[v\big(X_j(t)\big) - E_{\text{syn}}\big]; \tag{2.5}$$

here, $v(X_j)$ projects the vector X_j onto its corresponding voltage value, E_{syn} is a reversal potential, and $g_{\text{syn}}(X_k, t) \geq 0$ denotes the synaptic conductance that is activated by the action potential of neuron k. As long as the temporal dynamics of $g_{\text{syn}}(t)$ is short and does not violate assumption 3, equation 2.4 is a valid description for the smooth pulsatile synaptic transmission resulting from equation 2.5.

Remark 2. The coupling in the canonical θ-neuron network of theorem 1 is of pulse-response type $q(\theta_j)p(\theta_k)$ and reflects that weakly connected class 1 excitable neurons, equation 2.3, have type 1 phase response curves (PRC); for type 1 PRCs, positive (negative) inputs always lead to a positive (negative) phase shift of the postsynaptic neuron. In equation 2.4 the PRCs reduce to $q(\theta_j) = 1 + \cos\theta_j$. The type 1 property of the PRCs is inherited from the fact that each neuron is assumed to be ε^2-close to the SNIC bifurcation, and it is independent of the coupling function G_{jk}. Consequently, the pulses $p_{jk}(\theta_k)$ can indeed represent conductance-based synapses of the form 2.5. Relaxing the ε^2-closeness assumption will allow for also obtaining type 2 PRCs[2], which may entail very distinct synchronization properties of the network (see Smeal et al., 2010; Pazó & Montbrió, 2014).

In this article, I focus on pulses $p_{jk}(\theta) = s_{jk}p(\theta)$ with $p(\theta) \geq 0$ nonnegative. I will include no habituation, no delay or synaptic kinetics, no synaptic fatigue. My point here is to illustrate some of the consequences of the pulse function $p(\theta)$ on the network's collective behavior.

2.3 Voltage-Dependent Pulses of QIF Neurons. Equation 2.4 describes the dynamics of a network of θ-neurons with instantaneous pulse coupling, which has been rigorously derived from a universal class of weakly connected class 1 excitable neurons. Assuming weak interactions and homogeneous stereotypical action potential shapes, I now set $s_{jk} = J/N$ for all

[2] Note that in the proof of theorem 1, I approximated the phase θ_j in the function $p_{jk}(\theta_j, \theta_k) \approx p_{jk}(\theta_k)$ to be constant during an incoming spike see equation A15. This assumption breaks down if neuron j is no longer ε^2-close to the SNIC bifurcation and the PRC $\tilde{q}(\theta_j)$ has to be found from $\tilde{q}(\theta_j)\tilde{p}(\theta_k) = (1 + \cos\theta_j)p_{jk}(\theta_j, \theta_k)$.

$j, k = 1, \ldots, N$. Then, $p_{jk}(\theta_k) = Jp(\theta_k)/N$ with a general pulse function p and coupling strength $J \in \mathbb{R}$ rescaled with respect to the network size N. By identifying $v_j = \tan(\theta_j/2)$, the θ-neuron becomes equivalent to the QIF neuron (see Figures 1b and 1c; Ermentrout, 1996) and equation 2.4 can be transformed into a network model of QIF neurons, whose voltage variables v_j follow the subthreshold dynamics:

$$\frac{d}{d\tau} v_j = v_j^2 + \eta_j + \frac{J}{N} \sum_{k=1}^{N} p_k(\tau). \tag{2.6}$$

The pulses p_k received by postsynaptic neuron j,

$$p_k(\tau) = p\big(\theta_k(\tau)\big) = p\big(2 \arctan v_k(\tau)\big), \tag{2.7}$$

are then implicitly defined in terms of the presynaptic voltage v_k through the corresponding θ-phase. Because of the connection with the θ-model equation 2.4, the pulses p_k may already represent complex synaptic transmission through, for example, conductance-based synapses of the form $I_{\text{syn}} = g_{\text{syn}}(v_j, t)[E_{\text{syn}} - v_k(t)]$ (see equation 2.5). This pulse interpretation becomes rigorous due to the exact correspondence between QIF and θ-neurons when the QIF dynamics, equation 2.6, is equipped with a fire-and-reset rule that takes peak and reset potentials at infinity (see Figure 1). The equivalence with the θ-model is not the only raison d'être of the QIF model (see section 2.1), and there are alternative biologically plausible interpretations for pulses of finite width between interacting QIF neurons. In particular, the definition, equation 2.6, in terms of voltage variables v_j calls for an interpretation of equation 2.7 as voltage-dependent pulses independent from the derivation of the canonical pulse-coupled θ-model equation 2.4.

Remark 3. The QIF dynamics equation 2.6, were obtained through the forward transformation $v_j = \tan(\theta_j/2)$ from equation 2.4, where the θ-neuron represents the canonical model for a class 1 excitable neuron close to a SNIC bifurcation. As a matter of course, one can start with interacting QIF neurons and use the inverse transformation $\theta_j = 2 \arctan(v_j)$ to obtain a network model of θ-neurons as in equation 2.4, which does not necessarily represent the canonical model for class 1 neurons, as has been proposed in Börgers and Kopell (2005), and Kotani et al. (2014).

How can one introduce biologically plausible pulses of finite width between QIF neurons solely taking the QIF dynamics, equation 2.6, into account? Natural candidates are voltage-dependent pulses $p_k = p(v_k)$ that can be identified with the synaptic conductance $g_{\text{syn}}(v_k, t)$, where the presynaptic voltage acts instantaneously on g_{syn}, that is, $g_{\text{syn}}(v_k, t) = g_{\text{syn}}(v_k(t))$. Such an instantaneous relation has, for example, been manifested through the voltage-gated calcium influx at the presynaptic axon during an action

potential (Catterall, 2011) or through the sigmoidal relationship between neurotransmitter concentration and presynaptic voltage (Destexhe et al., 1994). One may additionally consider first- or higher-order synaptic kinetics of $g_{\text{syn}}(t)$ in response to a presynaptic pulse $p(v_k)$; for simplicity, however, I focus on instantaneous interactions (but see section 5.3). In conductance-based neuron models, instantaneous voltage-dependent pulses during synaptic transmission have frequently been described by sigmoidal functions of logistic[3] form,

$$s_\infty(v) = 1/\{1 + \exp[-(v - v_s)/k_s]\}, \tag{2.8}$$

with presynaptic voltage v and steepness and threshold parameters k_s and v_s (Ermentrout & Kopell, 1990; Wang & Rinzel, 1992; Destexhe et al., 1994; Golomb et al., 1996; Wang & Buzsáki, 1996; Ermentrout & Kopell, 1998; Kopell et al., 2000; Börgers, 2017). Exemplary pulse profiles for conductance-based Hodgin-Huxley-like neurons are shown in Figure 3 (see appendix B for details on the employed Wang-Buzsáki model). The pulse shape depends on the width of the action potential and on the slope k_s of the sigmoidal pulse function $s_\infty(v)$. Narrow action potentials and hard thresholds generate pulses that are almost symmetric about the spike time $t = 0$ (see the green pulse in Figure 3c1). Typically, however, pulses exhibit a fast rise shortly before and a slower decay after the spike (see the violet pulse in Figure 3c2).

QIF neurons, by comparison, have stereotyped and rather artificial action potentials (see Figure 4a). Using the sigmoidal pulse function $s_\infty(v)$, equation 2.8 leads to degenerate pulses that terminate sharply at the time of the spike (see Figure 4c1). To compensate for the hardwired artificial shape of the QIF's action potential, one can extend the pulses ad hoc and replace v by its absolute value $|v|$ (see the violet pulse function in Figure 4b2). This tactic generates pulses $p_\parallel(v) := s_\infty(|v|)$ that are symmetric about the spike time $t = 0$ (see the violet pulse in Figure 4c2). A symmetric pulse is a reasonable approximation of pulses in conductance-based neuron models with narrow action potentials and a sigmoidal function with a hard threshold $k_s \to 0$ (see the green pulse in Figure 3c1). For general asymmetric pulses as in Figure 3c, however, one has to come up with a different solution that breaks the symmetry of $p_\parallel(v)$ with respect to $v = 0$. For instance, one can combine two sigmoidal functions as

$$p_{\not\parallel}(v) = \frac{1}{1 + e^{(v - v_{s-})/k_{s-}}} + \frac{1}{1 + e^{-(v - v_{s+})/k_{s+}}} \tag{2.9}$$

[3] An alternative formulation of equation 2.8 uses the hyperbolic tangent, $t_\infty(v) = \{1 + \tanh[(v - v_t)/k_t]\}/2$, which coincides with $s_\infty(v)$ when choosing $v_s = v_t$ and $k_s = k_t/2$.

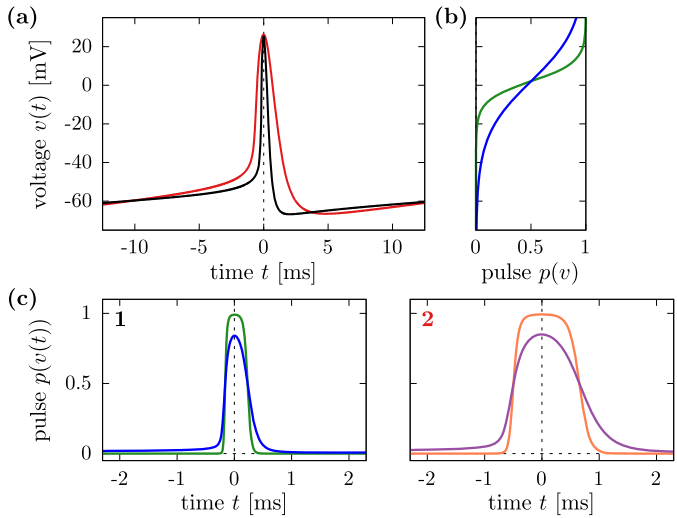

Figure 3: Voltage-dependent pulses of the conductance-based Wang-Buzsáki (WB) neuron. (a) Voltage traces of a periodically spiking WB neuron with narrow (black) or broad (red) action potentials (APs); both have frequency $f \approx 1/(24\text{ ms}) = 41.7$ Hz. (b) Sigmoidal pulse function, equation 2.8, with hard (green) and soft (blue) thresholds. The APs in panel a are transformed via panel b into pulses: (c1) a narrow AP and hard threshold result in a square-like pulse (green) that is symmetric about the spike time $t = 0$, whereas a soft threshold smooths and skews the pulse (blue); (c2) similar to panel c1 but for the wide AP. Parameters of pulses in panel b: $v_s = 2$ mV, $k_s = 5$ (green) as in Destexhe et al. (1994); $v_s = 2$ mV, $k_s = 14$ (blue).

with thresholds $v_{s+} > 0 > v_{s-}$ and steepness parameters $k_{s\pm} > 0$. For $k_{s+} < k_{s-}$, QIF neurons emit asymmetric pulses with a steep upstroke and a moderate downstroke (see the green pulse function in Figure 4b2 and the resulting pulse $p_{\text{⅄}}(v(t))$ in Figure 4c2).

2.4 An Accessible Family of Pulse Functions. In anticipation of an exact low-dimensional description for the collective dynamics of QIF neurons, it is advantageous to refrain from the explicit voltage dependence of the pulses, equation 2.9, and to formulate them in the corresponding θ-phase description (Pietras et al., 2023). This allows not only for a directly comparable treatment of networks of θ- and QIF neurons, but it also overarches the opposing approaches to pulse coupling introduced in sections 2.2 and 2.3; see also section 5.3.

By substituting $v = \tan(\theta/2)$ in equation 2.9, the voltage-dependent pulse $p_{\text{⅄}}(v)$ becomes phase dependent. However, the pulse $p_{\text{⅄}}(\tan(\theta/2))$ is only implicitly defined in θ, which hampers analytic tractability. As an

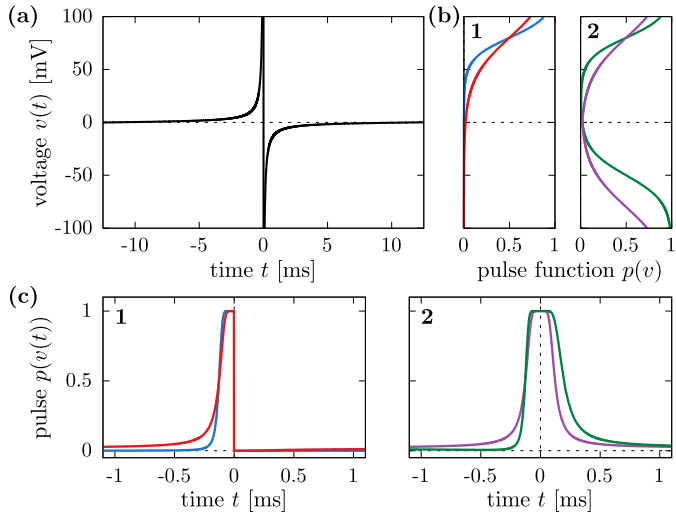

Figure 4: Voltage-dependent pulses of the QIF neuron. (a) Voltage trace of a periodically spiking QIF neuron with frequency $f \approx 41.7$ Hz. (b) Pulse functions consisting of (b1) one sigmoidal function as in Figure 3b or of (b2) a combination of two sigmoidals as in equation 2.9. (c1/c2), The action potential of the QIF neuron is transformed into the pulses using the pulse functions in b1, b2. Pulse parameters: (b1) equation 2.8 with $v_s = 80$ mV, $k_s = 10$ (blue) and $k_s = 20$ (red). (b2) $p_{\parallel}(v)$ with $v_s = 80$ mV, $k_s = 20$ (violet); $p_{\nparallel}(v)$ with $v_{s-} = -50$ mV, $k_{s-} = 12.5$, $v_{s+} = 80$ mV, $k_{s+} = 10$ (green).

alternative, I propose to use pulses $p(\theta)$ of the form 2.7 that start from the θ-phase description and a priori assume an implicit voltage dependence; in special cases the implicit voltage dependence can actually become explicit (see equation 2.11). Importantly, the explicit pulses, equation 2.9, can be approximated quite accurately around the resting potential by pulses $p(\theta) = p(2 \arctan v)$ that employ the θ-phase transformation of the QIF neuron (see Figure 5b).

Specifically, I propose the following family of accessible, analytically favorable, smooth pulse functions,

$$p_{r,\varphi,\psi}(\theta) = 1 + \frac{1 - r^2}{1 - r\cos\varphi} \frac{\cos(\theta - \psi - \varphi) - r\cos(\varphi)}{1 - 2r\cos(\theta - \psi) + r^2}, \tag{2.10}$$

which provide adequate approximations of the QIF pulses that can be symmetric about the spike time (see Figure 5c1) or asymmetric with a steep upstroke and a more moderate downstroke after the spike (see Figure 5c2). The shape of the pulses, equation 2.10, is determined by three parameters:

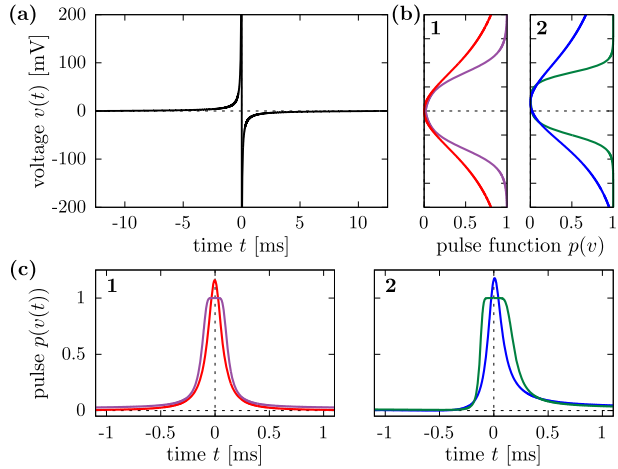

Figure 5: Smooth voltage-dependent pulses of (a) a periodically spiking QIF neuron with frequency $f \approx 41.7$ Hz. (b) The pulse functions, equation 2.9, shown in Figure 4b2 can be approximated around the resting potential by the phase-dependent pulse function equation 2.10 (red and blue traces; rescaled for convenience). The resulting smooth pulses (c) capture the nature of symmetric (c1) and asymmetric (c2) pulses quite accurately. Parameters for $p_{r,\varphi,\psi}(2\arctan v)/c$ are: (b1) $r = 0.985$, $\varphi = 0$, $\psi = \pi$, $c = 115$; (b2) $r = 0.985$, $\varphi = \pi/12$, $\psi = \pi$, $c = 35$.

$r \in [-1, 1]$, $\varphi \in [-\pi, \pi)$, and $\psi \in [0, 2\pi)$; $r < 1$ tunes the width of the pulse, $\varphi \neq 0$ tunes its asymmetry, and $\psi > \pi$ ($\psi < \pi$) shifts the pulse to the right (left) from the spike (at $\theta = \pi$). Crucially, these pulses admit an exact, low-dimensional description for the collective dynamics of globally coupled spiking neurons in terms of their firing rate and mean voltage (see section 3), and thus allow for a comprehensive mathematical analysis of how the pulse shape affects the synchronization properties of the network (see section 4).

To provide more details on the pulse functions, equation 2.10, first note that for $\varphi = 0$ and $\psi = \pi$, the equation reduces to a rectified-Poisson (RP) pulse, $p_{\mathrm{RP},r}(\theta) := p_{r,0,\pi}(\theta)$, with sharpness parameter $r \in (-1, 1)$ (Gallego et al., 2017). Via the transform $\theta = 2\arctan(v)$, one obtains the explicit voltage dependence of the RP pulse,

$$p_{\mathrm{RP},r}(v) = \frac{2(1-r)v^2}{(1+r)^2 + (1-r)^2 v^2}; \tag{2.11}$$

see Figures 5b1 and 5c1 for an example. The formulation in terms of the voltage v readily allows for using the pulses interchangeably in networks of θ- and QIF neurons. In the same manner, one can also obtain the general

voltage description of equation 2.10; as it is more convoluted, I refrain from presenting it here.

The RP pulse, equation 2.11, is a smooth generalization of the discontinuous δ-spike. When a neuron spikes and its voltage v diverges, then $\lim_{v\to\infty} p_{\mathrm{RP},r}(v) = 2/(1-r)$. Thus, in the limit $r \to 1$, $p_{\mathrm{RP},1}(v)$ becomes a Dirac δ-pulse and is zero except when v diverges. On the other hand, for $r \to -1$, $p_{\mathrm{RP},-1}(v) = 1$ is flat and the pulse is always "on" independent of the neuron's actual state. In the case $r = 0$, the RP pulse reads $p_{\mathrm{RP},0}(v) = 2v^2/(1+v^2)$, which corresponds to a cosine-pulse in the θ-phase description, $p_{\mathrm{RP},0}(\theta) = (1-\cos\theta)$.

Traditionally, cosine pulses have been generalized as Ariaratnam-Strogatz (AS) pulses according to Ariaratnam and Strogatz (2001),

$$p_{\mathrm{AS},n}(\theta) = a_n(1-\cos\theta)^n, \tag{2.12}$$

where $a_n = 2^n(n!)^2/(2n)!$ is a normalization constant and $n \in \mathbb{N}$ a sharpness parameter: for $n = 1$, one finds $p_{\mathrm{AS},1}(\theta) = p_{\mathrm{RP},0}(\theta)$; for $n \to \infty$, the AS pulse, equation 2.12, converges to a Dirac δ-pulse. AS pulses have been widely used in network models of θ-neurons (Goel & Ermentrout, 2002; Ermentrout, 2006; Luke et al., 2013, 2014; So et al., 2014; Laing, 2014, 2015, 2016a, 2016b; Roulet & Mindlin, 2016; Laing, 2017; Chandra et al., 2017; Laing, 2018a, 2018b; Aguiar et al., 2019; Lin et al., 2020; Laing & Bläsche, 2020; Laing & Omel'chenko, 2020; Means et al., 2020; Bläsche et al., 2020; Bick et al., 2020; Jüttner et al., 2021; Omel'chenko & Laing, 2022; Bîrdac et al., 2022), but suffer from numerical and also analytical difficulties when the pulses become more and more localized, $n \gg 1$. While RP pulses, equation 2.11, share the properties of AS pulses—they are symmetric about the pulse peak at $\theta = \pi$ and vanish at $\theta = v = 0$—, RP pulses overcome the numerical and analytical shortcomings of the AS pulse, equation 2.12, as will become clear below. In addition, the RP pulses can be readily extended to pulses that are skewed and/or whose peak is shifted away from $\theta = \pi$ (where $v = \tan(\theta/2)$ diverges) by introducing the asymmetry and shift parameters $\varphi \neq 0$ and $\psi \neq \pi$ in equation 2.10.

Pulses of the form of equation 2.10 satisfy some convenient analytic properties as they correspond to a rescaled Kato-Jones distribution (Kato & Jones, 2015). The Kato-Jones distribution is a four-parameter family of unimodal distributions on the circle, whose general form reads

$$p_{KJ}(\theta) = 1 + 2\,\mathrm{Re}\left\{C\sum_{n=1}^{\infty}(\xi e^{-i\theta})^n\right\} \tag{2.13}$$

with the complex-valued parameters $C = ae^{i\varphi}$ and $\xi = re^{i\psi} \in \mathbb{C}$. The Kato-Jones distribution, equation 2.13 generalizes the wrapped Cauchy distribution, which is obtained for $C \equiv 1$. One obtains equation 2.10 when setting

$a = (1 - r^2)/(2r)/(1 - r\cos\varphi) \geq 0$. This choice guarantees that the pulse is always nonnegative, $p_{r,\varphi,\psi}(\theta) \geq 0$, and vanishes at least once. Alternatively, one could reduce the number of parameters by enforcing equation 2.13 to vanish always at $\theta = 0$, which is in line with theorem 1 but may entail pulses that change signs. In this article, however, I focus on pulses $p(v) \geq 0$ so that the distinction whether the pulse coupling is excitatory or inhibitory is uniquely determined by (the sign of) the coupling strength J.

Taken together, the proposed family of pulses, equation 2.10, satisfies the properties: $p_{r,\varphi,\psi}(\theta)$ is 2π-periodic, nonnegative, unimodal, vanishes at least at one point, and has a normalized area in the course of an action potential, $\int_0^{2\pi} p_{r,\varphi,\psi}(\theta)d\theta = 2\pi$. Moreover, the pulses $p_{r,\varphi,\psi}(\theta)$ are smooth, except for the limit $r \to 1$, in which they converge to a Dirac δ-pulse,

$$p_{\delta,\psi}(\theta) := \lim_{r\to 1} p_{r,\varphi,\psi}(\theta) = 2\pi\delta(\theta - \psi). \tag{2.14}$$

The phase $\theta = \psi$, at which the δ-pulse is emitted, can be linked to a threshold voltage $v_{\text{thr}} = \tan(\psi/2)$ that, according to Ermentrout (1996), "accounts for the possibility that the synaptic conductance begins before the presynaptic voltage reaches its maximal value" (see also Gutkin et al., 2001). If $\psi > \pi$, then $v_{\text{thr}} < 0$ and the δ-pulse is emitted after the presynaptic voltage has reached its maximal value v_p and the neuron is recovering from the reset after its spike.

3 Exact Collective Dynamics of Globally Pulse-Coupled QIF Neurons

To determine the effect of the pulse shape on the collective network dynamics, I make use of a recently proposed exact reduction for globally coupled spiking neurons. I present the theory only for networks of QIF neurons, but the exact reduction equally holds for the corresponding θ-neuron dynamics (see appendixes C and D). Building on 2.6, I consider the membrane potentials v_j of QIF neurons $j = 1, \ldots, N$, that follow the subthreshold dynamics (Izhikevich, 2007; Ermentrout, 1996; Latham et al., 2000),

$$\tau_m \dot{v}_j = v_j^2 + I_0 + I_{\text{syn}} + I_j. \tag{3.1a}$$

The membrane time constant τ_m is typically of the order $\tau_m = 10$ ms, I_0 is a global input common to all neurons, I_{syn} a global recurrent synaptic input to be defined below, and I_j describes neuron-specific, independent inputs,

$$I_j(t) = \gamma[c\,\eta_j + (1 - c)\xi_j(t)], \tag{3.1b}$$

comprising heterogeneous and noisy inputs; $c\gamma$ determines the degree of heterogeneity; and $(1 - c)\gamma$ is the noise intensity. Quenched heterogeneity

η_j (as in equation 2.6) is sampled from a normalized Cauchy-Lorentz distribution. $\xi_j(t)$ describes independent Cauchy white noise with $\langle \xi_j(t) \rangle_t = 0$ and $\langle \xi_j(t)\xi_k(s) \rangle_t = \delta_{j,k}\delta(t-s)$. The parameter $c \in [0,1]$ in equation 3.1b weighs the relative deterministic and stochastic contributions to I_j on the microscopic level, but does not have an impact on the macroscopic dynamics (Clusella & Montbrió, 2022; Pietras et al., 2023). The subthreshold dynamics, equation 3.1, is complemented by a fire-and-reset mechanism: upon reaching a threshold v_p, the voltage v_j is reset to the potential v_r and neuron j is said to elicit a spike. Spike times T_j of neuron j are defined implicitly by $v_j(T_j) = v_p$. As the quadratic term in equation 3.1 causes the voltage to diverge in finite time, I consider $v_p = -v_r = \infty$, so that the QIF neuron is equivalent to the θ-model (Ermentrout, 1996) when identifying the voltage v_j with a phase θ_j via the transformation $v_j = \tan(\theta_j/2)$; neuron j spikes when θ_j crosses π (see Figure 1).

The spike times $T_j^{k=1,2,\dots}$ of neurons $j = 1, \dots, N$ allow for linking the theoretical model, equation 3.1, with experimental observations via the population activity commonly defined in terms of the firing rate,

$$R_N(t) = \lim_{\tau_r \to 0} \frac{1}{N} \sum_{j=1}^{N} \sum_k \frac{1}{\tau_r} \int_{t-\tau_r}^{t} \delta(t - T_j^k) dt, \tag{3.2}$$

where the subscript N indicates the network size and τ_r is a small time window over which to sum spikes. The firing rate R is at the heart of mean-field models in computational neuroscience, whose ultimate goal is to provide a self-consistent, at best exact (i.e., matching an underlying microscopic network model), dynamic description of the population activity that is closed in a few macroscopic variables. A singular example for such an exact mean-field model was proposed by Montbrió et al. (2015) for QIF neurons (see Luke et al., 2013, and Laing, 2014, for previous work on the related θ-neurons, yet without providing an explicit differential equation for the firing rate $R(t)$). Montbrió et al.'s approach yielded ordinary differential equations that describe the dynamics of the firing rate R and the mean voltage $V = \langle v_j \rangle = \frac{1}{N}\sum_{j=1}^{N} v_j$. A major success of Montbrió et al.'s firing rate equations was to pinpoint a spike synchronization mechanism through the cooperative interplay between the neurons' voltage and firing dynamics that is central for collective network oscillations, inherent in almost all neuron network models, but not captured by traditional firing rate models by default. In the following, I employ a reduction strategy that builds on the ideas in Montbrió et al. (2015) and is developed further in Pietras et al. (2023).

3.1 Firing Rate and Voltage (RV) Dynamics. A remarkable feature of the globally coupled QIF neurons described by equation 3.1 is that their

collective dynamics is captured by a low-dimensional system of differential equations (Montbrió et al., 2015; Pietras et al., 2023). The low-dimensional description becomes exact in the thermodynamic limit of infinitely many neurons, $N \to \infty$, which I adopt from now on. The macroscopic state of the QIF network is then given by the probability density function $\mathcal{W}(v,t)$, so that $d\mathcal{W}(v,t)dv$ indicates the fraction of neurons with membrane potential in the interval $[v, v+dv)$ at time t. Correspondingly, in the θ-phase description, one can formulate the probability density $\mathcal{P}(\theta,t)$ with variable $\theta = 2\arctan(v)$. The latter distribution density can be expanded in Fourier space as $\mathcal{P}(\theta,t) = (2\pi)^{-1}\{1 + \sum_{n\geq 1} Z_n(t)e^{-in\theta} + c.c.\}$, where the modes $Z_n(t)$ are the Kuramoto-Daido order parameters (Kuramoto, 1984; Daido, 1996) and their dynamics are given in appendix D. The two characteristic observables of neural networks—the firing rate R and mean voltage V—can conveniently be expressed as

$$\pi\tau_m R - iV = 1 + 2\sum_{n=1}^{\infty}(-1)^n Z_n = \Phi + \lambda\frac{\mathcal{M}(-\sigma)}{\sigma}, \tag{3.3}$$

where $\Phi(t), \lambda(t), \sigma(t)$ are complex-valued variables and $\mathcal{M}(k)$ is a constant function that depends on the initial distribution $\mathcal{W}(\theta, t=0)$ of the QIF neurons. As detailed in Pietras et al., 2023 (see also appendix D), the dynamics of the three complex variables $\Phi, \lambda, \sigma \in \mathbb{C}$ are governed by

$$\tau_m\dot{\Phi} = i\Phi^2 - iI(t) + \gamma, \quad \tau_m\dot{\lambda} = 2i\Phi\lambda, \quad \tau_m\dot{\sigma} = i\lambda, \tag{3.4}$$

where $I(t) = I_0 + I_{\text{syn}}(t)$; note that the macroscopic dynamics equation 3.4, are independent of the parameter c in equation 3.1b. In the presence of Cauchy white noise and/or Cauchy-Lorentz heterogeneity, $\gamma > 0$, $\lambda \to 0$ asymptotically in time (Pietras et al., 2023), and the collective dynamics becomes uniquely determined by $\Phi \to \pi\tau_m R - iV$ or, equivalently, by the firing rate R and the mean voltage V. More precisely, the collective dynamics converges to an invariant two-dimensional manifold (Ott & Antonsen, 2008; Luke et al., 2013; Montbrió et al., 2015), also called the Lorentzian manifold $\{\lambda = 0\}$, which contains all possible attractors of the full six-dimensional dynamics, equation 3.4 and is given by the time-dependent total voltage density of the QIF neurons in form of a Cauchy-Lorentz distribution with mean $V(t)$ and half-width $\pi\tau_m R(t)$ (Montbrió et al., 2015),

$$\mathcal{W}(v,t) = \frac{1}{\pi}\frac{\pi\tau_m R(t)}{[v - V(t)]^2 + [\pi\tau_m R(t)]^2}. \tag{3.5}$$

For the analysis of asymptotic regimes, it suffices to restrict the focus on the firing rate and voltage (RV) dynamics on the invariant Lorentzian manifold, which can be guaranteed by initializing the voltages $v_j(0)$ according to a

Cauchy-Lorentz distribution.[4] Setting $\lambda \equiv 0$ in equations 3.3 and 3.4 leads to the RV dynamics on the Lorentzian manifold (Montbrió et al., 2015; Pietras et al., 2023; Clusella & Montbrió, 2022),

$$\tau_m \dot{R} = \frac{\gamma}{\pi \tau_m} + 2RV, \tag{3.6a}$$

$$\tau_m \dot{V} = V^2 - (\pi \tau_m R)^2 + I_0 + I_{\text{syn}}, \tag{3.6b}$$

which exactly describes the collective dynamics of large pulse-coupled networks of QIF neurons, equation 3.1. In the next step, I incorporate smooth pulsatile synaptic transmission mediated by the pulses (see equation 2.10) and show how the global recurrent current I_{syn} can be expressed in terms of the macroscopic variables R and V, which leads to an exact mean-field model that is closed in the population firing rate R and mean voltage V.

3.2 Recurrent Synaptic Input in the RV Dynamics. Montbrió et al. (2015) considered QIF neurons that interacted with each other in a global (all-to-all) and instantaneous fashion through δ-spikes, that is, by emitting Dirac δ-pulses at their spike times T_j^k. Then, I_{syn} in equations 3.1 and 3.6 becomes proportional to $\tau_m R(t)$ as given by equation 3.2. However, the δ-spike assumption for recurrent, instantaneous coupling is particularly limiting (Afifurrahman et al., 2021) not only for biological but also for numerical reasons[5] (Catllá et al., 2008; Klinshov et al., 2021; Feketa et al., 2021) and also because the limit of infinitely narrow pulses does not commute with the thermodynamic limit of infinitely large networks (Zillmer et al., 2007; Montbrió et al., 2015) nor does it allow for collective oscillations (Montbrió et al., 2015; Ratas & Pyragas, 2016; Jüttner et al., 2021). Here, I avoid those difficulties by modeling interneuronal communication with smooth pulses of finite width that unfold in the course of an action potential of presynaptic neuron j in a similar manner as neurotransmitters are released in response to the depolarization of the voltage v_j (see section 2.3).

For globally coupled QIF neurons, the recurrent input $I_{\text{syn}}(t) = \langle s_j(t) \rangle$ is the population mean over all individual postsynaptic responses $s_j(t)$ to a pulse $p_j(t)$ emitted by presynaptic neuron j. As discussed above, I consider voltage-dependent, smooth pulses $p_j(t) = p\big(\theta_j(t)\big) = p\big(2 \arctan v_j(t)\big)$ with the pulse function $p(\theta) = p_{r,\varphi,\psi}(\theta)$ given by equation 2.10. The θ-phase formulation of the pulses guarantees analytic tractability thanks to favorable properties of the corresponding probability density $\mathcal{P}(\theta, t)$ of the ensemble

[4] For different choices of initial conditions $\{v_j(0)\}_j$, one has to resort to the full six-dimensional dynamics equation 3.4 and define $\mathcal{M}(k)$ appropriately (see Pietras et al., 2023).

[5] Dirac δ-pulse interactions $\dot{x}(t) = f(t, x(t)) + g(t, x(t))\delta(t - t_0)$ for some functions f and g should be understood throughout this article as $\dot{x}(t) = f(t, x(t))$ for $t \neq t_0$ and $x(t_0^+) = x(t_0^-) + g(t_0, x(t_0^-))$ at $t = t_0$ (see Feketa et al., 2021).

of θ-neurons (Pietras et al., 2023), but does not limit the generality of results for general voltage-dependent pulses. Moreover, the pulses of equation 2.10 allow for a smooth approximation of δ-spikes, equation 2.14, with $\psi = \pi$. Summing over all neurons $j = 1, \dots, N$, yields the connection to the firing rate R in equation 3.2 as:

$$P_{N,\delta} := \frac{1}{N}\sum_{j=1}^{N} p_{\delta,\pi}(\theta_j) = \frac{2\pi}{N}\sum_{j=1}^{N}\frac{\delta(t-T_j^k)}{2/\tau_m} = \pi\tau_m R_N, \tag{3.7}$$

where the first equality follows from the change of variables formula for Dirac δ-functions: $\delta(t-T_j^k) = \delta\big(g(t)\big)\big|\dot{g}(T_j^k)\big|$ with $g(t) = \theta_j(t) - \pi$ and $\dot{g}(T_j^k) = \dot{\theta}_j(T_j^k) = 2/\tau_m$. The sum over the spike times T_j^k is taken within a short time window of length τ_r as in equation 3.2.

Equation 3.7 explicitly links the mean presynaptic pulse activity $P_{\delta,\pi} = \langle p_{\delta,\pi}\rangle$ to the firing rate R (see also equation E3). Ironically, the δ-spike assumption again conceals an even deeper connection: in the thermodynamic limit $N \to \infty$, the mean pulse activity $P_{r,\varphi,\psi}$ is fully determined by the firing rate $R(t)$ *and* the mean voltage $V(t)$. The description of $P_{r,\varphi,\psi}$ in terms of R and V becomes explicit on the Lorentzian manifold, where

$$\begin{aligned} P_{r,\varphi,\psi}(t) &= \big\langle p_{r,\varphi,\psi}\big(\theta_j(t)\big)\big\rangle = \lim_{N\to\infty}\frac{1}{N}\sum_{j=1}^{N} p_{r,\varphi,\psi}\big(\theta_j(t)\big) \\ &= \int_0^{2\pi} p_{r,\varphi,\psi}(\theta)\mathcal{P}(\theta,t)d\theta = P_{r,\varphi,\psi}\big(R(t),V(t)\big). \end{aligned}$$

In general, $P_{r,\varphi,\psi}$ depends on R and V only through the three complex variables Φ, λ, σ (see equation F.1 in appendix F) but on the Lorentzian manifold $\{\lambda = 0\}$, it reduces to

$$P_{r,\varphi,\psi}(R,V) = \mathrm{Re}\,(\Psi) \quad \text{where} \quad \Psi = \frac{(1-r^2)(1+\pi\tau_m R - iV)e^{-i\varphi} + (r-\cos\varphi)\big[1 - re^{-i\psi} + (\pi\tau_m R - iV)(1+re^{-i\psi})\big]}{r(1-r\cos\varphi)\big[1-re^{-i\psi} + (\pi\tau_m R - iV)(1+re^{-i\psi})\big]} \tag{3.8}$$

(see appendixes E to G for a rigorous derivation). Albeit complex in its general description in terms of R and V as well as of the parameters r, φ and ψ, equation 3.8 dramatically simplifies for certain pulse shapes.

For RP pulses $p_{\mathrm{RP},r} = p_{r,0,\pi}$ (see equation 2.11) that are symmetric ($\varphi = 0$) about the peak phase when the neuron spikes ($\psi = \pi$), the mean presynaptic pulse activity $P_{\mathrm{RP},r} = \langle p_{\mathrm{RP},r}\rangle = P_{r,0,\pi}$ reads:

$$P_{\mathrm{RP},r}(R,V) = \frac{2\pi\tau_m R[1+r+(1-r)\pi\tau_m R] + 2(1-r)V^2}{[1+r+(1-r)\pi\tau_m R]^2 + (1-r)^2V^2}. \tag{3.9}$$

Taking the limit $r \to 1$, yields the mean activity of δ-spikes, $\lim_{r\to 1} P_{r,0,\pi} = \pi\tau_m R$, which coincides with the population firing rate as already shown in equation 3.7.

Dirac δ-pulses do not necessarily need to be emitted at the instant a neuron spikes (when $v \to \infty$), but when v crosses a virtual threshold voltage $v_{\rm thr} < \infty$. The corresponding peak phase is $\psi = 2\arctan(v_{\rm thr})$ and the mean presynaptic activity $P_{\delta,v_{\rm thr}} := \langle p_{\delta,2\arctan(v_{\rm thr})}\rangle$ for pulses of the form 2.14 becomes

$$P_{\delta,v_{\rm thr}}(R,V) = \frac{\pi\tau_m R(1+v_{\rm thr}^2)}{(\pi\tau_m R)^2 + (V - v_{\rm thr})^2}. \tag{3.10}$$

Importantly, for the general family (see equation 2.10) of pulse functions $p_{r,\varphi,\psi}$, the mean presynaptic pulse activity, equation 3.8, explicitly depends on the mean voltage V, that is, $\partial_V P_{r,\varphi,\psi} \neq 0$, except for the limit $(r,\varphi,\psi) \to (1,0,\pi)$. As I show in section 4.1, it is exactly this voltage dependence that is crucial for collective oscillations in case of instantaneous pulse coupling. The emergent macroscopic oscillations, however, are sensitive to the pulse shape: skewing the pulses slightly to the phase after the spike yields robust collective oscillations of inhibitory neurons, which are not present for symmetric pulse coupling (see Figure 6). A thorough analysis how the pulse shape affects network synchronization is the focus of section 4. To anticipate, for RP pulses that are symmetric about the peak phase $\theta = \pi$, collective oscillations are restricted to a narrow and rather unrealistic region in parameter space. By contrast, for (asymmetric) pulses with their peak phase after the actual spike, $\theta > \pi$, collective oscillations emerge almost naturally in inhibitory networks ($J < 0$) with excitatory input currents ($I_0 > 0$). This is a strong reminder of interneuronal network gamma (ING) oscillations in inhibitory networks, including synaptic kinetics with finite rise and decay times (Wang & Buzsáki, 1996; Brunel & Hakim, 1999; Brunel & Wang, 2003).

As a wrap-up, I have presented an exact low-dimensional description for globally pulse-coupled QIF neurons (see equation 3.1) in the thermodynamic limit, which equally holds for networks of θ-neurons (see equation C5). For pulses $p_{r,\varphi,\psi}$ of the general form (2.10), the mean pulse activity $P_{r,\varphi,\psi} = \langle p_{r,\varphi,\psi}\rangle$ can conveniently be expressed in terms of the macroscopic variables. The time-asymptotic macroscopic dynamics of the QIF neurons is restricted to the invariant Lorentzian manifold, on which the collective behavior is exactly described by the RV dynamics, equation 3.6. For instantaneous pulse coupling, one has to substitute

$$I_{\rm syn} = JP_{r,\varphi,\psi}(R,V) \tag{3.11}$$

in equation 3.1, where J indicates the pulse-coupling strength and the mean pulse activity $P_{r,\varphi,\psi}$ is given by equation 3.8. The RV dynamics, equation 3.6,

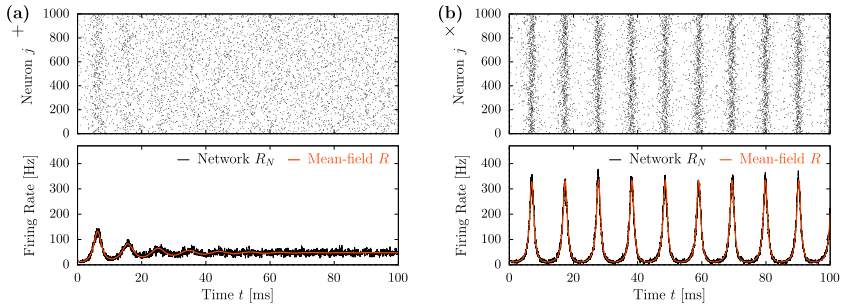

Figure 6: Collective dynamics of inhibitory QIF neurons globally coupled via instantaneous pulses $p_{r,\varphi,\psi}$ with $r = 0.95$ and $\psi = \pi$. (a) Symmetric RP pulses ($\varphi = 0$, red curve in Figure 7a) drive the network into an asynchronous state. (b) Asymmetric pulses slightly skewed to the phase after the spike ($\varphi = \pi/12$, red curve in Figure 8a) yield robust ING oscillations. Top: Raster plots show spike times of 1000 QIF neurons obtained from network simulations according to equation 3.1 with $N = 10{,}000$ neurons. Bottom: Excellent agreement between firing rates R_N (black) and R (orange) obtained from integrating the QIF network and the RV dynamics (see equation 3.6) with equations 3.9 and F6 for panels a and b, respectively. Network parameters are $\gamma = 1$, $I_0 = 20$, $J = -12$ (see $+$ in Figure 7c4 and $\times$ in Figure 8d). The membrane time constant is $\tau_m = 10$ ms. Network simulations were performed using Euler-Maruyama integration with $dt = 5 \cdot 10^{-3}$ ms, and the firing rate R_N was computed using equation 3.2 with $\tau_r = 10^{-1}$ms.

is two-dimensional and closed in two macroscopic variables—the firing rate R and the mean voltage V.

The reduction of the RV dynamics greatly facilitates the investigation how the pulse shape affects collective dynamics of pulse-coupled spiking neurons, as the mean-field (see equation 3.6) accurately reproduce the microscopic network dynamics (see equation 3.1) of globally coupled QIF neurons with instantaneous pulses $p_{r,\varphi,\psi}$ (see Figure 6).

Initial voltages $v_j(0)$ of the microscopic network were chosen to follow a Cauchy-Lorentz distribution of half-width $R(0)$ and centered at $V(0)$ for an immediate match between network and RV simulations. For arbitrary initial conditions, one has to resort to the six-dimensional dynamics (see equations 3.3 and 3.4) with a properly chosen constant function $\mathcal{M}(k)$ for such a perfect agreement (see Pietras et al., 2023).

In the following, I capitalize on the fact that the reduced RV dynamics, equation 3.6, perfectly captures network simulations of pulse-coupled spiking neurons and analyze them with respect to emergent collective behavior for various choices of the pulse function, equation 2.10. In doing so, I also show that the collective dynamics in Figure 6 can be predicted by linear stability analysis (see the $+$ in Figure 7c4 and $\times$ in Figure 8d below). The main

focus of section 4 lies on voltage-mediated synchronization in general and on collective oscillations in inhibitory networks, in particular, with instantaneous pulses whose peak occurs at the time of the presynaptic spike or shortly thereafter.

4 Collective Oscillations with Instantaneous Pulses

Networks of inhibitory interneurons provide a mechanism for coherent brain oscillations, particularly in the gamma band, as reciprocal inhibition turned out to be effective for neuronal synchrony (Wang, 2010). For class 1 excitable neurons, such as θ-neurons or the QIF model equation 3.1, collective oscillations—as a hallmark of synchrony—can be realized even with relatively fast inhibitory synapses (Ermentrout, 1996). Synaptic latency (including axonal delay) as well as rise and decay times contribute to determining synchronous firing patterns (Van Vreeswijk et al., 1994; Wang & Buzsáki, 1996; White et al., 1998; Brunel & Wang, 2003; Maex & De Schutter, 2003; Brunel & Hansel, 2006; Wang, 2010). Exact RV dynamics corresponding to equation 3.6 have been successfully employed to describe collective oscillations of inhibitory QIF neurons interacting via δ-spikes with first-order (Devalle et al., 2017; Dumont & Gutkin, 2019) and second-order synaptic kinetics (Byrne et al., 2017; Coombes & Byrne, 2019; Clusella, Köksal-Ersöz et al., 2022) or with delay (Pazó & Montbrió, 2016; Ratas & Pyragas, 2018; Devalle et al., 2018; for extensions, see also: Keeley et al., 2019; Byrne et al., 2020, 2022; di Volo & Torcini, 2018; Bi et al., 2020; di Volo et al., 2022; and Avitabile et al., 2022). For instantaneous synapses, however, δ-spike-interactions do not allow for macroscopic oscillations (Montbrió et al., 2015; Jüttner et al., 2021), whereas instantaneous pulses of finite width have been reported to induce collective oscillations in inhibitory networks of the equivalent θ-neurons (Luke et al., 2013; So et al., 2014; Laing, 2015; Lin et al., 2020; Jüttner et al., 2021) interacting via symmetric AS pulses, equation 2.12. For globally coupled QIF neurons with (nonsmooth) pulses of finite width, collective oscillations have so far only been found in excitatory networks (see Ratas & Pyragas, 2016, equation 29).

In this section, I systematically study how the pulse shape affects collective oscillations in the two-dimensional RV dynamics, equation 3.6, with instantanteous pulse coupling. I focus on identifying the transitions from asynchronous to synchronous collective behavior upon varying the coupling strength J and the mean input I_0. Mathematically speaking, I will perform bifurcation analysis of macroscopic stationary (asynchronous) states and characterize stability changes when varying control, or bifurcation, parameters. When the asynchronous state loses stability and gives rise to collective oscillations (synchrony), these oscillations can be distinguished right at their onset having either (1) small amplitude and finite frequency, (2) high amplitude and finite frequency, or (3) high amplitude and arbitrarily low frequency. Cases 1 and 2 correspond to a so-called Hopf bifurcation that is

either super- or subcritical; case 3 corresponds to a SNIC or a homoclinic bifurcation. The simplest scenario and quite common for collective oscillations to emerge is a supercritical Hopf bifurcation. The other cases require bistability of multiple steady states, and one typically finds saddle-node bifurcations close by.

Before exploring the bifurcation structure of the collective dynamics for particular pulse shapes, I first prove in section 4.1 that the RV dynamics, equation 3.6, with instantaneous synaptic transmission can generate collective oscillations through a Hopf bifurcation only if the recurrent synaptic input explicitly depends on the mean voltage V. Such an effective voltage-coupling occurs for pulses of finite width, equation 3.9, but also for Dirac δ-pulses emitted before or after, but not at, the presynaptic spike, equation 3.10. However, for symmetric RP pulses, as I show in section 4.2, collective oscillations are feasible in only a small range of inhibitory coupling ($J < 0$) and mean inputs $I_0 > 0$, limited by Hopf and homoclinic bifurcation boundaries. For asymmetric right-skewed pulses, the bifurcation structure simplifies and yields collective oscillations for a large range of inhibitory coupling and positive mean inputs (see section 4.3), substantiating the notion of Figure 6b that narrow pulses slightly skewed to the phase after the spike are a promising candidate for generating ING oscillations. For completeness, I investigate the onset of collective oscillations for left-skewed pulses in section 4.4, though they are biologically less plausible and require recurrent excitation instead of inhibition.

4.1 Collective Oscillations through Voltage Coupling. The collective dynamics for networks of globally coupled spiking neurons with instantaneous synaptic transmission is exactly described by the RV dynamics, equation 3.6. On the Lorentzian manifold, the RV dynamics is two-dimensional and closed in the firing rate R and mean voltage V as the recurrent synaptic input $I_{\text{syn}}(t)$ depends instantaneously, and smoothly, on R and V, that is, $I_{\text{syn}}(t) = I_{\text{syn}}(R(t), V(t))$. The onset of collective oscillations via a Hopf bifurcation can be determined using the eigenvalues

$$\lambda_{1,2} = \frac{1}{2}\left[\text{tr(Jac)} \pm \sqrt{\text{tr(Jac)}^2 - 4\text{det(Jac)}}\right]$$

of the Jacobian of the RV dynamics, equation 3.6,

$$\text{Jac} = \begin{pmatrix} 2V^* & 2R^* \\ -2\pi^2\tau_m^2 R^* + \partial_R I^*_{\text{syn}} & 2V^* + \partial_V I^*_{\text{syn}} \end{pmatrix}, \tag{4.1}$$

evaluated at the fixed-point solution (R^*, V^*) with

$$V^* = -\gamma/(2\pi\tau_m R^*) \quad \text{and} \quad I^*_{\text{syn}} = I_{\text{syn}}(R^*, V^*); \tag{4.2}$$

the Jacobian equation 4.1 is obtained in rescaled time $\tilde{t} = \tau_m t$, and $\partial_x = \partial/\partial x$ with $x \in \{R, V\}$. By definition 3.2, the firing rate $R \geq 0$ is nonnegative such that the fixed-point solution (R^*, V^*) satisfies $V^* \leq 0$ because of equation 4.2; the inequality becomes strict for $\gamma > 0$.

A Hopf bifurcation of the fixed point (R^*, V^*) occurs if $\mathrm{tr(Jac)} = 0$ and $\det(\mathrm{Jac}) > 0$. From $\mathrm{tr(Jac)} = 0$, one has $\partial_V I^*_{\mathrm{syn}} = -4V^*$. Since $V^* < 0$ is negative for $\gamma > 0$, the necessary condition for collective oscillations in equation 3.6 emerging through a Hopf bifurcation of the fixed point (R^*, V^*) reads:

$$\partial_V I^*_{\mathrm{syn}} := \partial_V I_{\mathrm{syn}}(R^*, V^*) > 0. \tag{4.3}$$

That is, collective oscillations require recurrent coupling through the mean voltage V. Put differently, if the recurrent synaptic input I_{syn} is independent of V, that is, $\partial_V I^*_{\mathrm{syn}} = 0$, then equation 4.3 cannot be satisfied for any fixed-point solution $(R^*, V^*) \in \mathbb{R}^+ \times \mathbb{R}^-$, and the network of globally coupled QIF neurons will not synchronize.

To show that collective oscillations are indeed possible if the first condition, $\mathrm{tr(Jac)} = 0$ is satisfied, it is necessary to prove that the second condition, $\det(\mathrm{Jac}) > 0$, can also be satisfied. Assuming that $\mathrm{tr(Jac)} = 0$ holds and using the fixed-point equation in equation 4.2 one obtains

$$\det(\mathrm{Jac}) = (2\pi\tau_m R^*)^2 - \frac{\gamma^2}{(\pi\tau_m R^*)^2} - \frac{4\gamma}{\pi\tau_m}\frac{\partial_R I^*_{\mathrm{syn}}}{\partial_V I^*_{\mathrm{syn}}}.$$

By assumption, $I_{\mathrm{syn}}(R, V)$ is smooth, so for $\partial_V I^*_{\mathrm{syn}} > 0$, the right-hand side is well behaved and can be expressed as a smooth function in R^*. While $\det(\mathrm{Jac}) < 0$ for small firing rates $R^* \to 0$ (e.g., due to strong inhibitory input $I_0 \ll 0$) the determinant $\det(\mathrm{Jac})$ will become positive for large firing rates $R^* \gg 1$ (and/or for $\partial_R I^*_{\mathrm{syn}} \ll 0$). As $R^* = R^*(I_0)$ depends smoothly on the external current I_0—the functional dependence of R^* on I_0, that is, the transfer function or fI-curve, can be obtained by setting the right-hand side of equation 3.6b to zero and inserting equation 4.2 (see also Devalle et al., 2017), one can expect that for strong excitatory drive, $I_0 \gg 1$, R^* increases sufficiently such that both conditions, $\mathrm{tr(Jac)} = 0$ and $\det(\mathrm{Jac}) > 0$, are simultaneously satisfied and give rise to collective oscillations.

Hence, only if the recurrent synaptic input I_{syn} explicitly depends on the mean voltage V can collective oscillations in the RV-dynamics, equation 3.6, emerge through a Hopf bifurcation from a fixed-point solution (R^*, V^*) with sufficiently large firing rate $R^* \gg 0$. In other words, an asynchronous, typically high-activity state becomes unstable through an effective voltage coupling and the spiking neurons start firing synchronously (as in Figure 6b).

Now, when does the recurrent input I_{syn} explicitly depend on the mean voltage V? This occurs naturally for electrical coupling through gap

junctions (see Pietras et al., 2019, and Section 5.2). In the absence of gap junctions and as shown in section 2.3, an effective voltage coupling can also be achieved with instantaneous pulses that are different from Dirac δ-pulses emitted at the presynaptic spike (see also Ratas & Pyragas, 2016). For instantaneous pulses $p_{r,\varphi,\psi}$ given by equation 2.10, the synaptic current $I_{\text{syn}}(t) = JP_{r,\varphi,\psi}(R, V)$ depends explicitly on the voltage V (see equation 3.8) and thus generally allows for collective oscillations of globally coupled QIF neurons; one can achieve that equation 4.3 holds true by freely tuning the coupling strength J. Whether collective oscillations occur in realistic parameter regimes, for example, with global inhibition $J < 0$ and excitatory drive $I_0 > 0$, crucially depends on the pulse-shape parameters r, φ, ψ, as I demonstrate in sections 4.2 to 4.4.

To anticipate whether particular pulse shapes $p_{r,\varphi,\psi}$ require excitatory or inhibitory coupling for neural synchronization, one can compute $\partial_V P_{r,\varphi,\psi}(R, V)$ and recall that any fixed-point solution (R^*, V^*) satisfies $R^* > 0$ and $V^* < 0$ for $\gamma > 0$. Then, for RP pulses, equation 2.11, one has

$$\partial_V P_{\text{RP},r}(R^*, V^*) = \frac{4(1-r^2)[1+r+(1-r)\pi\tau_m R^*]V^*}{\left\{[1+r+(1-r)\pi\tau_m R^*]^2 + (1-r)^2 V^{*2}\right\}^2} < 0. \quad (4.4)$$

Thus, to satisfy condition 4.3, $J\partial_V P_{\text{RP},r}(R^*, V^*) > 0$, RP pulses require inhibitory coupling ($J < 0$) to generate collective oscillations. For shifted Dirac δ-pulses, equation 2.14, the sign of

$$\partial_V P_{\delta,\text{thr}}(R^*, V^*) = \frac{2\pi\tau_m R^*(v_{\text{thr}} - V^*)(1+v_{\text{thr}}^2)}{[(\pi\tau_m R^*)^2 + (V^* - v_{\text{thr}})^2]^2} \quad (4.5)$$

depends on the virtual threshold value v_{thr}. If a neuron emits the Dirac δ-pulse shortly after its spike (i.e., when it is recovering from its reset, $v \leftarrow -\infty$), then $v_{\text{thr}} < 0$ and $\partial_V P_{\delta,\text{thr}}(R^*, V^*) < 0$, so collective oscillations occur for inhibitory coupling ($J < 0$). If the pulse is emitted before the neuron spikes, then $v_{\text{thr}} \gg 0$, $\partial_V P_{\delta,\text{thr}}(R^*, V^*)$ can become positive, and collective oscillations require excitatory coupling ($J > 0$). For other pulse shapes, it is more laborious to draw similar conclusions from $\partial_V P_{r,\varphi,\psi}(R^*, V^*)$ alone. However, the general trend, which will become clear in section 4.2 to 4.4, is that collective oscillations occur with inhibitory coupling when the mean of the pulse $p_{r,\varphi,\psi}(\theta)$ coincides with the spike or is shifted to its right, whereas pulses whose mean is shifted to the left of the spike require excitatory coupling to synchronize the network.

4.2 Rectified-Poisson (RP) Pulses ($\varphi = 0, \psi = \pi$). For symmetric pulses ($\varphi = 0$) of finite width ($r < 1$) centered around the spike threshold ($\psi = \pi$), the mean pulse activity $P_{\text{RP},r}$ is given by equation 3.9. In Figure 7a,

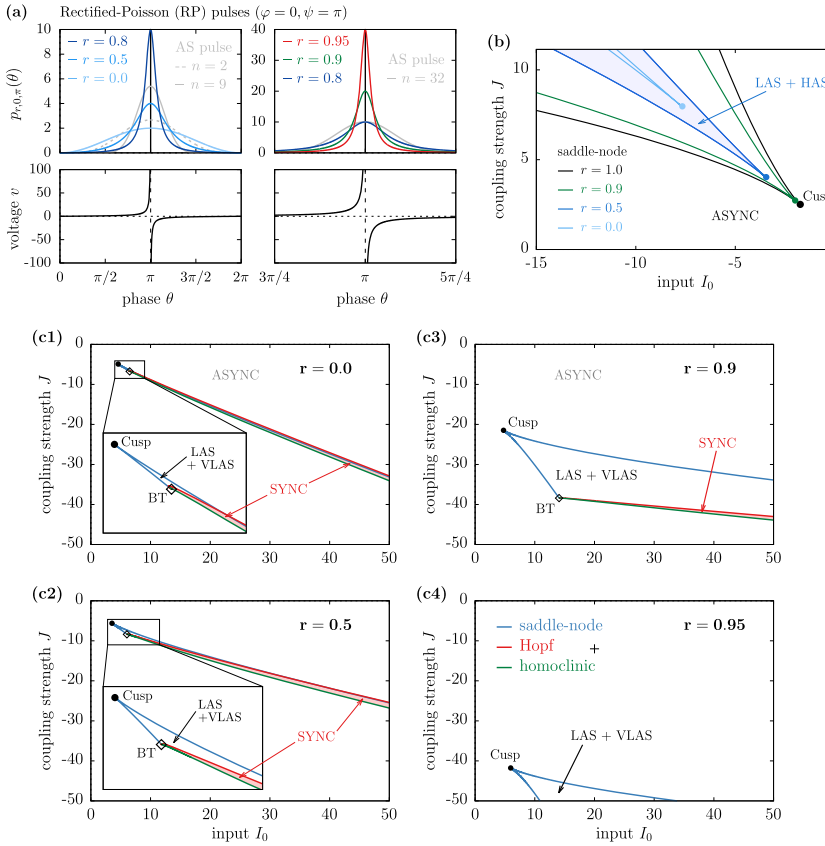

Figure 7: Phase diagrams of the RV dynamics, equation 3.6, for instantaneous RP pulses. (a) Comparison of pulse profiles: RP pulses of various width $r \leq 1$ (color coded) are symmetric about the peak phase $\theta = \pi$ corresponding to the instant where the voltage v diverges; see the bottom panels for the link between v and the theta-phase $\theta = 2\arctan(v)$. The larger $r \nearrow 1$, the narrower the pulse (note the different x-axis-scale in the right panel). AS pulses (see equation 2.12) with different width parameters $n \in \mathbb{N}$ are shown in grey for comparison. The RP pulse with $r = 0$ coincides with $p_{\mathrm{AS},1}$. (b) Bistability between low and high activity, asynchronous states (L/HAS) in excitatory networks ($J > 0$). Saddle-node bifurcation boundaries are color-coded according to the pulse width r of the RP pulses shown in panel a. (c1–4) Collective oscillations in narrow parameter regions (red, SYNC) for inhibitory networks ($J < 0$) and decreasing pulse width $r = 0, 0.5, 0.9, 0.95$. Insets in panels c1–2 zoom in on the general bifurcation structure near the Bogdanov-Takens (BT) point, where saddle-node (blue), (supercritical) Hopf (red), and homoclinic (green) bifurcation curves meet. The $+$ in panel c4 denotes the parameters used for numerical simulations in Figure 6a.

it can be appreciated that the smaller $r < 1$, the wider the RP pulse (see equation 2.11) about the peak phase π at which the presynaptic voltage diverges (bottom panel). The shape of the RP pulses (color coded for different r) is similar to AS pulses (see equation 2.12) (grey). The major advantage of RP pulses is that $P_{\mathrm{RP},r}$ is a simple function in R and V (see equation 3.9) whereas no such closed form exists for arbitrary AS pulses with shape parameter $n \in \mathbb{N}$ (see appendixes E and F). It is thus straightforward to perform linear stability analysis of the RV dynamics, equation 3.6, with RP pulses, but not with arbitrary AS pulses. All bifurcation boundaries can be obtained analytically, except for that of the homoclinic, which is a global bifurcation and has to be determined numerically (Doedel et al., 2007; Gast et al., 2019). In the following, I set $\gamma = 1$ and refrain from a denormalization with respect to γ as it would affect the mean pulse activity $P_{r,\varphi,\psi}$ in a nontrivial way; for different choices of $\gamma > 0$, I have not noticed any qualitative differences.

For excitatory coupling ($J > 0$), RP pulses are not capable of generating collective oscillations, as expected for reasonable parameter choices and as predicted by equation 4.4. Instead, the cusp-shaped region in Figure 7b features bistability between two asynchronous states: a low-activity state (LAS) and a high-activity state (HAS). In line with the results for δ-spikes by Montbrió et al. (2015), the narrower the RP pulse ($r \nearrow 1$), the bigger the cusp-shaped region of bistability until it finally coincides with the one found for $r = 1$ (black); the boundaries of the bistability regions are SN bifurcations and meet at a codimension-2 bifurcation point (Cusp).

For inhibitory networks ($J < 0$) with positive input currents ($I_0 > 0$) (see Figure 7c) the asynchronous steady state loses stability at a supercritical Hopf bifurcation (red curve), where collective oscillations arise with small amplitude. With increasing $|J|$ (i.e., stronger inhibition), the amplitude of the collective oscillations grows, whereas their frequency decreases up to the critical point at the green curve, where the frequency becomes zero and collective oscillations are destroyed; this critical point is called a homoclinic bifurcation. The red-shaded region between the red and the green curve, where collective oscillations exist and neurons spike in synchrony (that is why this region is labeled SYNC), occurs for limited values of inhibition only. Similar results were obtained by Jüttner et al. (2021) for the case $r = 0$ and by Luke et al. (2013) and Lin et al. (2020) for wide AS pulses ($n = 2, 9$). There is also a region of bistability between an LAS and a very low-activity state (VLAS), bounded by the (blue) saddle-node curve, that meets the Hopf and homoclinic curves at the BT point, another codimension-2 bifurcation. For larger r (i.e., for narrower pulses), this BT point moves farther down so that collective oscillations require strong inhibitory coupling $J \ll 0$. On top of that, collective oscillations remain confined to a narrow region in parameter space, which becomes almost negligible for RP pulses that are reasonably localized with $r > 0.8$ (see Figures 7c3 and 7c4).

4.3 Right-Skewed Pulses ($\varphi > 0$ and/or $\psi > \pi$)**.** Shifting ($\psi \neq \pi$) and/or skewing ($\varphi \neq 0$) the symmetric RP pulses critically affects the collective dynamics of globally coupled QIF neurons. By introducing a virtual threshold $v_{\text{thr}} = \tan(\psi/2)$ at which the emitted pulse is strongest, one can shift the pulse to the right ($\psi > \pi$) or to the left ($\psi < \pi$) of the QIF threshold v_p at infinity (see Figure 8a, blue curve); note that $v_{\text{thr}} \to v_p = \infty$ for $\psi \to \pi$. By introducing an asymmetry parameter $\varphi \neq 0$, one can skew the pulse (see Figure 8a, red and green curves). Asymmetric pulses $p_{r,\varphi,\psi}(\theta)$ do not take on their maximum at $\theta = \psi$ when v diverges and the neuron spikes, but their peak is shifted to the right ($\varphi > 0$) or to the left ($\varphi < 0$) of the spike. Though the peak shift is rather small,[6] the mean of the pulse moves clearly away from the threshold phase $\psi = 2\arctan(v_{\text{thr}})$; see the vertical red-dashed line in Figure 8a.

As before, one can perform linear stability analysis of the RV dynamics, equation 3.6, now with mean presynaptic input $P_{r,\varphi,\psi}$ given by equation 3.8 for general pulses, equation 2.10. As motivated in section 2.3, I will focus on pulses $p_{r,\varphi,\psi}$ whose mean is shifted to the right of the spike, that is, $\varphi > 0$ and/or $\psi > \pi$. In Figure 8b, I shift the narrow RP pulse ($r = 0.95$, red in Figure 7a) such that it reaches its peak when the presynaptic voltage crosses the virtual threshold $v_{\text{thr}} = -20$ when recovering from the reset after its spike. This shift immediately affects the SYNC region of collective oscillations: While the SYNC region literally falls out of view for narrow RP pulses (with $v_{\text{thr}} = \infty$), for shifted RP pulses the SYNC region moves closer to $J = 0$ and grows as the homoclinic bifurcation curve (green) is pushed away from the Hopf curve (red). Shifting the pulse thus facilitates neuronal synchrony. Although the bifurcation structure appears more involved, the effect on the collective dynamics is small. The following technical details can hence be skipped; I report them here only for completeness. The cusp-shaped region of bistability between the LAS and the VLAS grows into the ($I_0 < 0$)-region—albeit with negligible effects on the overall dynamics because the VLAS has a diminutive basin of attraction (not shown)—and the upper saddle-node curve (blue) coincides with the homoclinic curve beyond the saddle-node-separatrix-loop (SNL) bifurcation point. The violet curve to the right of the SNL point denotes a saddle-node on invariant circle (SNIC) bifurcation that terminates the collective oscillations. Furthermore, the supercritical Hopf bifurcation (red solid) becomes subcritical (red dashed) at a generalized Hopf (GH) bifurcation point, from which a saddle node of cycles (SN of cycles) bifurcation curve (orange) emanates (see the inset in Figure 8b). In the red region bounded by the supercritical Hopf/SN

[6] An asymmetric pulse $p_{r,\varphi,\psi}$ with $\varphi \neq 0$ and $\psi = 2\arctan(v_{\text{thr}})$ has its peak when the presynaptic neuron's voltage v reaches $v_{\max} = \frac{(1+r)v_{\text{thr}}\cos(\varphi/2)+(1-r)\sin(\varphi/2)}{(1+r)\cos(\varphi/2)-(1-r)v_{\text{thr}}\sin(\varphi/2)}$, and the pulse vanishes at $v_{\min} = \frac{(1+r)v_{\text{thr}}\sin(\varphi/2)-(1-r)\cos(\varphi/2)}{(1+r)\sin(\varphi/2)+(1-r)v_{\text{thr}}\cos(\varphi/2)}$. The corresponding peak and trough phases θ can be found via $\theta_{\max\,/\,\min} = 2\arctan(v_{\max\,/\,\min})$.

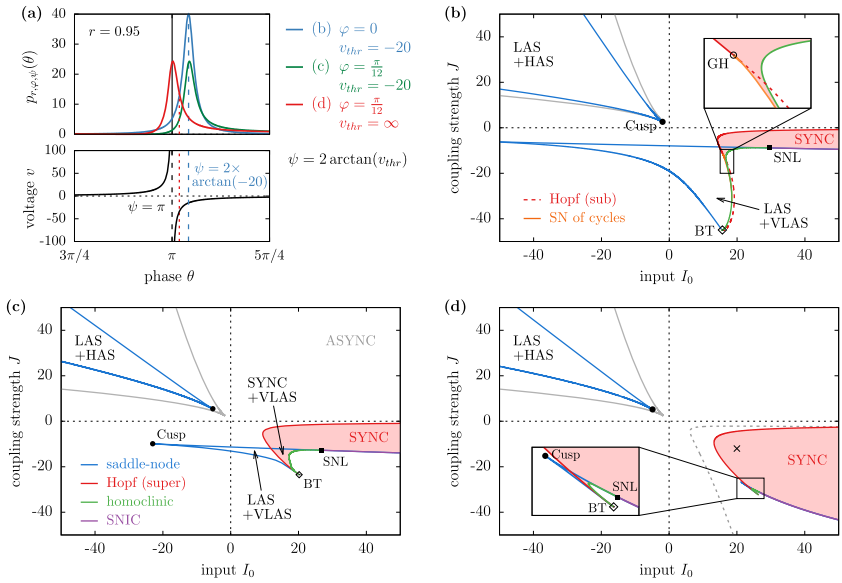

Figure 8: Phase diagrams of the RV dynamics, equation 3.6, for right-skewed pulses. (a) Comparison of pulse profiles that are shifted (blue; $\varphi = 0, \psi = -2\arctan 20$), asymmetric (red; $\varphi = \pi/12, \psi = \pi$) or both (green; $\varphi = \pi/2, \psi = -2\arctan 20$); pulse width is $r = 0.95$. The mean of the shifted pulse coincides with its peak phase $\theta = \psi$ (blue dashed), whereas the mean of the asymmetric pulse (red dotted) is shifted to the right of its peak. (b–d) Phase diagrams of the collective dynamics for pulses shown in panel a. Collective oscillations are found in the red shaded regions (SYNC) for inhibitory coupling ($J < 0$) and excitatory drive ($I_0 > 0$). Asymmetric pulses yield larger SYNC regions, while bistability regions (between low-activity states (LAS) or collective oscillations and very low-activity states (VLAS)) are drastically reduced. Boundaries for codimension 1-bifurcations are colored lines: saddle node (blue), supercritical Hopf (red solid), subcritical Hopf (red dashed), homoclinic (green), SNIC (violet), saddle node of cycles (orange). Codimension 2-bifurcation points are marked by symbols: cusp (circle), Bogdanov-Takens (BT, diamond), saddle-node separatrix loop (SNL, square). In panel d, the $\times$-symbol denotes the parameter values for numerical simulations in Figure 6b and the gray dashed curve is the supercritical Hopf boundary for the RV dynamics, equation 5.10 with first-order synaptic kinetics, $\tau_m = 2\tau_d = 10\,\text{ms}$, $\tau_r = 0\,\text{ms}$, in the limit of δ-spikes $(r, \varphi, \psi) \to (1, 0, \pi)$.

of cycles curve and the homoclinic curve, there is bistability between the VLAS and SYNC; that is, the LAS loses stability and gives rise to collective oscillations at the Hopf bifurcation. For excitatory coupling ($J > 0$), on the other hand, shifting the RP pulse hardly affects the cusp-shaped region of bistability between the LAS and the HAS.

Introducing small right-skewed asymmetry ($\varphi > 0$) allows for an even broader parameter region of collective oscillations, while simplifying the bifurcation scenario to great extent. In Figure 8c, I consider pulses that are both shifted ($v_{\text{thr}} = -20$) and skewed ($\varphi = \pi/12$); see the green pulse in Figure 8a. The Hopf bifurcation is now always supercritical and the bistability region between LAS and VLAS shrinks drastically, whereas the bistability region between the VLAS and SYNC is only slightly increased. Compared to the case $\varphi = 0$, the bistability region between LAS and HAS also shrinks for $J > 0$.

In Figure 8d I consider only skewed, but not shifted, pulses $p_{0.95,\pi/12,\pi}$ to disentangle the effect of the asymmetry from that of the shift parameter. For large $r = 0.95$ and small $|\varphi| \ll 1$, an individual pulse (red curve in Figure 8a) reaches its maximum for $v_{\max} = (r+1)/(r-1)/\tan(\varphi/2)$ almost immediately after the presynaptic spike at $\theta = \pi$. However, the asymmetry parameter φ shifts the bulk of the pulse, and hence its mean, farther away from π, which has a nontrivial effect on the collective dynamics: one may have expected an overall picture of the collective dynamics to be somewhere in between that of nonshifted and shifted RP pulses; yet the skewed pulse dramatically enhances the SYNC regime of collective oscillations that dominates the parameter region for $J < 0$ and $I_0 > 0$. Moreover, the bistability regions within the triangle of cusp, SNL, and BT points become almost negligible. This scenario strongly resembles the case for synaptic dynamics with a dominant SYNC region bounded by a supercritical Hopf bifurcation (Devalle et al., 2017; Clusella, Köksal-Ersöz et al., 2022). In fact, if one considers first-order synaptic dynamics $\tau_d \dot{S} = -S + P_{r,\varphi,\psi}$ with synaptic decay time constant $\tau_d > 0$, collective oscillations emerge already for δ-spike-interactions, $(r, \varphi, \psi) \to (1, 0, \pi)$. Consistent with the literature (Devalle et al., 2017), collective oscillations always emerge via a supercritical Hopf bifurcation (see Figure 8d, dashed grey line). Noteworthy, the parameter regions of collective oscillations almost coincide for instantaneous asymmetric pulses and for synaptic kinetics triggered by δ-spikes.

4.4 Left-Skewed Pulses ($\varphi < 0$ and/or $\psi < \pi$). For biological plausibility, I previously considered pulses whose mean coincided with the QIF threshold at infinity or was shifted to the neuron's refractory phase after the spike (i.e., the mean of the pulse had a phase $\theta_{\text{mean}} \geq \pi$). For completeness, I briefly report on pulses whose mean is advanced to the phase before the spike. The red curve in Figure 9a describes a left-skewed pulse that I obtained from mirroring the asymmetric red pulse in Figure 8a by setting $\varphi = \pi/12 \mapsto -\pi/12$ while keeping $r = 0.95$ and $\psi = \pi$ (i.e., $v_{\text{thr}} = \infty$) as before. The mean is now shifted to the left (the dashed line indicates the spike at $\theta = \psi$), which changes the phase diagram drastically (compare Figure 9b with Figure 8d). First, the synchronous state of collective oscillations (SYNC) does not exist for recurrent inhibition but requires

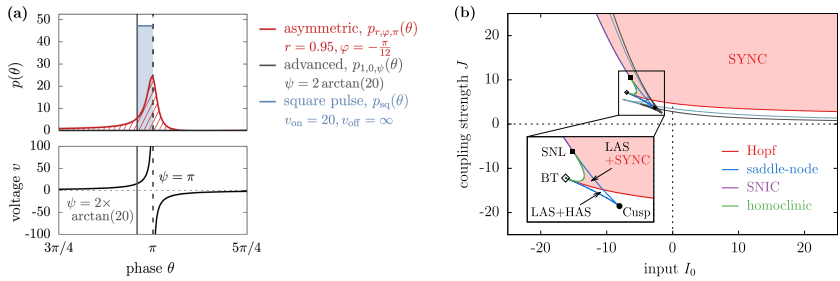

Figure 9: Left-skewed pulses induce collective oscillations for excitatory, but not for inhibitory neurons. (a) Asymmetric (red), advanced (dark gray) and square pulses (gray-blue), whose mean lies to the left of the QIF threshold at $\theta = \pi$, where the voltage v diverges (bottom). (b) The phase diagram using the asymmetric pulse $p_{r,\varphi,\pi}$ exhibits a dominant region for collective oscillation (SYNC, red shaded), which is bounded by a supercritical Hopf bifurcation curve (red) from below and by a SNIC (violet) and homoclinic (green) bifurcation from the left. In the triangular region between the Bogdanov-Takens (BT), saddle-node separatrix loop (SNL), and cusp points, there is bistability between a high-activity (HAS) and a low-activity asynchronous state (LAS) below, and between the LAS and SYNC in the red-shaded region above the Hopf curve; see the inset for a zoom. The dark-gray and gray-blue lines correspond to the phase diagram structure of the advanced and the square pulses depicted in panel a.

excitation ($J > 0$). Then the cusp-shape bifurcation region that dominated the upper left part ($J > 0, I_0 < 0$) in Figures 7 and 8 has shrunk to a small triangular region bounded by the three codimension-2 bifurcation points (BT, SNL, and cusp, see the inset in Figure 9b). The Hopf bifurcation line emanating from the BT point separates the triangular bistability region into a lower part, where two asynchronous states (a low- and a high-activity state) coexist, and an upper part, where the high-activity asynchronous state (HAS) has lost stability and given rise to collective oscillations. Overall, the phase diagram strongly resembles the case of gap junction coupling in interplay with δ-spikes (see Figure 7 of Pietras et al., 2019).

What is more, the shape of left-skewed pulses has little impact on the phase diagram. For advanced Dirac δ-pulses $p_{\delta,\psi}(\theta)$, equation 2.14, with $\psi = 2\arctan(v_{\mathrm{thr}}) < \pi$, see the dark gray curve in Figure 9a with virtual threshold $v_{\mathrm{thr}} = 20$, the phase diagram is only slightly shifted downward and the triangular bistability region has become a bit smaller (dark gray lines in Figure 9b).

For comparison, I also consider square pulses $p_{\mathrm{sq}}(v)$ similar to those considered by Ratas and Pyragas (2016),

$$p_{\mathrm{sq}}(v) = \begin{cases} \pi/\vartheta, & \text{if } v \geq v_{\mathrm{on}} \text{ or } v \leq v_{\mathrm{off}}, \\ 0, & \text{otherwise}, \end{cases} \tag{4.6}$$

where $\vartheta := (\theta_{\text{off}} - \theta_{\text{on}})/2$ with onset and offset phases $\theta_{\text{off,on}} = 2\arctan(v_{\text{off,on}})$ is chosen such that the square pulse p_{sq} in the corresponding θ-phase description is normalized to 2π (see section 2.4). For $v_{\text{off}} \to -\infty$ and $v_{\text{on}} > 0$, equation 4.6 coincides with the pulses used by Ratas and Pyragas (2016), but rescaled by π/ϑ; see the blue pulse in Figure 9a with $v_{\text{on}} = 20$ for an example. For $v_{\text{on}} > 0$ and $v_{\text{off}} < 0$, the square pulse p_{sq} does not terminate at the spike, but actually encloses it and extends its impact to the neuron's relative refractory period.

To obtain the mean pulse activity $P_{\text{sq}} = \langle p_{\text{sq}} \rangle$, it is no longer possible to follow the approach of section 3.2 because the pulses $p_{\text{sq}}(v)$ do not possess the desired mathematical properties; in particular, they do not permit an analytic continuation in the complex plane. Nonetheless, it is possible to obtain the RV dynamics for global square-pulse coupling on the Lorentzian manifold. To this end, one can average the square pulses, equation 4.6, with respect to the Cauchy-Lorentz distribution density $\mathcal{W}(v, t)$, equation 3.5, which results in the mean presynaptic pulse activity:

$$\begin{aligned} P_{\text{sq}}(R, V) &= \int_{-\infty}^{\infty} p_{\text{sq}}(v)\mathcal{W}(v, t)dv \\ &= \frac{1}{\vartheta}\left[\arctan\left(\frac{V - v_{\text{on}}}{\pi\tau_m R}\right) - \arctan\left(\frac{V - v_{\text{off}}}{\pi\tau_m R}\right)\right]. \end{aligned} \tag{4.7}$$

For $v_{\text{off}} \to -\infty$, equation 4.7 reduces to the global synaptic variable used by Ratas and Pyragas (2016) rescaled with π/ϑ.

Equation 4.7 can readily be used for the recurrent input $I_{\text{syn}} = JP_{\text{sq}}$ in the RV dynamics, equation 3.6. Linear stability analysis for square pulses with $v_{\text{on}} = 20$ and $v_{\text{off}} = \infty$ (blue pulse in Figure 9a) yields a very similar phase diagram compared to the asymmetric and advanced pulses; see the gray-blue lines in Figure 9b and see Ratas and Pyragas (2016): A large parameter region of collective oscillations occurs in the upper right quadrant for excitatory coupling $J > 0$, which could have been anticipated along the same lines as in section 4.1 because $\partial_V P_{\text{sq}}(R^*, V^*) = \pi\tau_m R^*/\vartheta/[(\pi\tau_m R^*)^2 + (V^* - v_{\text{on}})^2] > 0$ for all fixed-point solutions $R^* > 0$.

In sum, left-skewed pulses, which may be biologically less plausible because their mean effect occurs before the neuron actually spikes, do not allow for collective oscillations among inhibitory QIF neurons, but only among excitatory neurons, and, the resulting phase diagram is largely insensitive to the shape of the pulse, which is in stark contrast to symmetric RP pulses (see Figure 7) and right-skewed pulses (see Figure 8).

5 Discussion

The motivation for the work at hand has been to include and justify another degree of biological realism—namely, smooth pulsatile synaptic

transmission—within the framework of an exact and low-dimensional mean-field theory for networks of globally coupled spiking neurons (Montbrió et al., 2015; Pietras et al., 2023). The resulting RV dynamics, equation 3.6, are admissible to mathematical analysis and allow for comprehensive insights into how the pulse shape affects the collective dynamics. Unless considering synaptic interaction via δ-spikes, previous studies on pulse-coupled spiking θ-neuron networks typically resorted to broad, symmetric, and rather inflexible Ariaratnam-Strogatz (AS) pulses, equation 2.12, more for mathematical convenience than for biological realism (see section 2.2). The main reason for using AS pulses seems a historic one. To provide some context, I review previous approaches to pulse coupling between θ-neurons in section 5.1. Here, I also revisit an alternative approach to pulse coupling between QIF neurons, which has led to biologically contradictory results on the single neuron as well as on the network level, and which is restricted to the Lorentzian manifold.

To overcome previous limitations and analyze the effect of biologically plausible pulse shapes—both symmetric and asymmetric—on the collective dynamics of globally pulse-coupled QIF and θ-neurons (even beyond the Lorentzian manifold), I have proposed a rather general family of pulse functions $p_{r,\varphi,\psi}(\theta)$, equation 2.10, that depend on the presynaptic voltage v via their θ-phase description $\theta(t) = 2\arctan(v(t))$. In the limit $(r, \varphi, \psi) \to (1, 0, \pi)$, the pulse reduces to the δ-spike commonly used in network models of spiking neurons. Taking the mean over those δ-spikes yields a direct connection with the population firing rate, $\langle p_{1,0,\pi} \rangle = \pi \tau_m R$ (see equation 3.7). Tuning either of the three pulse parameters—its width r, asymmetry φ, and shift ψ—allows for diverse pulse shapes $p_{r,\varphi,\psi}$ that may mimic realistic synaptic transmission between pre- and postsynaptic neurons and, by adjusting the timing of the synapse, crucially influence the collective dynamics of the network. I have concentrated on nonnegative pulses, equation 2.10, only and could therefore reduce the number of parameters of the analytically tractable Kato-Jones pulses, equation 2.13, from four to three. In section 5.2, I discuss these three pulse parameters in more detail and draw connections to delay and electrical coupling via gap junctions. When loosening the modeling assumptions, such as the closeness to a SNIC bifurcation in theorem 1, the more general Kato-Jones pulses, equation 2.13, that change signs can also be thought possible as an extension of equation 2.10, studying their effects on the collective dynamics will be left for future work. In view of more general synaptic processes, I discuss in section 5.3 whether instantaneous pulses of finite width can replace more complex synaptic transmission, such as synaptic kinetics and conductance-based synapses, beyond the interpretation inherent in theorem 1. Recall that theorem 1 imposed certain constraints on the pulse width in order to establish the θ-neuron network, equation 2.4, and its QIF-equivalent, equation 2.6, as the canonical pulse-coupled network model for weakly connected class 1 excitable neurons. For the discussion in section 5.3, I discard those

restrictions on the pulse function p. Instead, I regard the θ-model as the continuous analogue of the (discontinuous) QIF model (see remark 3). In this way, the pulses $p_{r,\varphi,\psi}(\theta)$ in the θ-neuron network, equation 2.4, can be probed against the hypothesis that they may, or may not, correspond to complex synaptic interactions in the QIF network, equation 3.1.

5.1 Previous Approaches to Pulse Coupling. The phase representation of the θ-neuron suggests invoking the theory of coupled phase oscillators to study synchronization and emergent collective behavior. Yet insights from the literature on pulse coupling in related phase models may not always carry over to θ-neurons, and one ought to be careful when drawing analogies. Revisiting the arguments that justified pulses of finite width between coupled phase oscillators will lead to the root of the "pulse problem" in θ-neurons. To this end, I consider a network of N globally coupled neurons described by variables $\theta_j \in \mathbb{S}^1$, $j = 1, \ldots, N$, with the dynamics

$$\dot{\theta}_j = \omega_j - b_j \cos(\theta_j) + \frac{1}{N} \sum_{k=1}^{N} q(\theta_j) p(\theta_k). \tag{5.1}$$

The network dynamics, equation 5.1, reduces to the network model, equation 2.4, of θ-neurons for $\omega_j = 1 + \eta_j$, $b_j = 1 - \eta_j$ and $q(\theta) = 1 + \cos(\theta)$ with excitability parameter η_j. More generally, equation 5.1 describes the dynamics of active rotators (Shinomoto & Kuramoto, 1986; Kuramoto et al., 1987) with pulse-response coupling; $p(\theta_k)$ is a pulse-like function, and $q(\theta_j)$ plays a role analogous to that of a "phase response curve" (Winfree, 1980). The parameter b_j determines whether neuron j is periodically spiking ($|\omega_j| > b_j$) or in an excitable regime ($|\omega_j| \leq b_j$). Setting $b_j = 0$ for all j leads to the seminal Winfree model (Winfree, 1967, 1980).

In the context of neural oscillators, Ermentrout & Kopell (1990) used the Winfree model—equation 5.1 with $b_j = 0$—to describe the dynamics of periodically firing neurons (with frequency ω_j) on their limit cycle, parameterized by the phase θ_j. In the course of an action potential, the presynaptic neuron k emits a pulse $p(\theta_k)$ that is modulated by the response function $q(\theta_j)$ of postsynaptic neuron j. For Hodgkin-Huxley-like neurons, the pulses $p(\theta)$ can be interpreted as instantaneous nonlinear conductances (Ermentrout & Kopell, 1990; Wang & Rinzel, 1992). By using graded potentials rather than fast spikes, synaptic interaction in these kinetics-based models is represented as a function of the presynaptic voltage. Analogously, in kinetic models of synaptic transmission, the neurotransmitter concentration in the synaptic cleft can be reduced to a sigmoidal function of the presynaptic voltage (Destexhe et al., 1994; see also: Koch, 2004; Ermentrout & Terman, 2010; Rothman, 2013). According to these theories, a voltage-dependent pulse can comprise the biochemical processes—at the presynaptic site—from the initiation of an action potential until the release of neurotransmitters

to the synaptic cleft. The resulting pulse can become arbitrarily broad and typically exhibits a steep increase until the neuron spikes and a moderate decrease afterward (Ermentrout & Kopell, 1990). Its asymmetric shape results from the interplay between the action potential shape and the synaptic activation, or neurotransmitter release, function. Asymmetric pulses were shown to be critical to synchronization in neural networks consisting of two neurons (Wang & Rinzel, 1992; Skinner et al., 1994; Sato & Shiino, 2007); a comprehensive picture how asymmetric pulses affect the collective behavior of large neural networks, however, has been lacking.

The argumentation that pulses $p(\theta)$ in the Winfree model result from the interplay between action potential shape and synaptic activation function may justify the use of broad pulses also in networks of θ-neurons. This reasoning ignores, however, that the trajectory of an action potential in conductance-based neurons is radically compressed in the canonical θ-model (see Figure 1) so the resulting pulse cannot become arbitrarily broad (see Figure 2). Besides, the Winfree model describes the phase dynamics of periodically firing conductance-based neurons obtained through a proper phase reduction (Ermentrout & Kopell, 1990), whereas the θ-neuron (albeit a phase model) does not result from phase reduction. Instead, it canonically describes a particular dynamical regime of a neuron that does not need to be periodically spiking but can also be excitable. Hence, adopting the Winfree model, equation 5.1, with $b_j = 0$, with broad and possibly asymmetric pulses $p(\theta)$ for networks of θ-neurons has to be regarded with care. Still, as long as θ-neurons are in the periodically firing regime, the Winfree model may be useful for studying their collective dynamics, at least to some extent (Hoppensteadt & Izhikevich, 1997; Izhikevich, 1999; Clusella, Pietras et al., 2022), and previous results about the effect of the response and pulse functions $q(\theta_j)$ and $p(\theta_k)$ on synchronization properties in the Winfree model can become applicable (Ariaratnam & Strogatz, 2001; Pazó & Montbrió, 2014; Gallego et al., 2017).

To account for excitable neuronal dynamics, the Winfree model has to be augmented by a term proportional to $\cos(\theta_j)$, yielding the network model equation 5.1, of coupled active rotators. A thorough analysis of this equation with general pulse and response functions p and q is lacking, though. So far, building on Kuramoto et al. (1987), O'Keeffe and Strogatz studied how the width of (symmetric) pulses affects the collective dynamics, while considering a flat response function $q \equiv const$ and identical $b_j = b$ (O'Keeffe & Strogatz, 2016). They found that broad pulses may entail collective dynamics different from those generated by narrow pulses, which is consistent with results on the Winfree model by Pazó & Montbrió (2014) and Gallego et al. (2017). It remains unclear, however, how these results carry over to θ-neuron networks, including sinusoidal response functions and excitable dynamics.

A crucial tool for pinpointing the effect of the pulse width on the synchronization properties of large populations of Winfree oscillators and active

rotators has been an exact dimensionality reduction first proposed by Ott and Antonsen (2008). Since then, a plethora of studies have adopted the "Ott-Antonsen ansatz" to facilitate mean-field analyses. But to do so, they had to rely on analytically tractable pulse and response functions, for example, resorting to symmetric and broad pulses as suggested by Ariaratnam and Strogatz (2001), and thus often at the cost of biological realism. By that time, the Ariaratnam-Strogatz (AS) pulse had already found its way into networks of θ-neurons (Goel & Ermentrout, 2002; Ermentrout, 2006) as a mathematical tractable alternative to similar, mainly symmetric, pulses of finite width (see, e.g., Gutkin et al., 2001; Osan & Ermentrout, 2001; Börgers & Kopell, 2003, 2005; Kömek et al., 2012; Gutkin, 2014), which were introduced either for numerical convenience (to smooth the discontinuous δ-spikes) or on the premise that instantaneous pulse coupling reflected realistic synaptic potentials. Typically, however, the authors did not specify which synaptic processes they meant to replace by broad pulses. In section 5.3, I reexamine their premise and argue that pulses, irrespective of their (finite) width, cannot reflect real synaptic dynamics—at the postsynaptic site—and ought not to be used to replace synaptic transmission with synaptic kinetics or conductance-based synapses in networks of spiking neurons. Regardless, the combination of the Ott-Antonsen ansatz with the analytically tractable, though biologically debatable, AS pulses turned out to be pivotal to studying the collective dynamics of pulse-coupled θ-neurons (Luke et al., 2013, 2014; So et al., 2014; Laing, 2014, 2015, 2016a, 2016b, 2017, 2018a, 2018b; Roulet & Mindlin, 2016; Chandra et al., 2017; Aguiar et al., 2019; Lin et al., 2020; Laing & Bläsche, 2020; Laing & Omel'chenko, 2020; Means et al., 2020; Bläsche et al., 2020; Bick et al., 2020; Jüttner et al., 2021; Omel'chenko & Laing, 2022; Bîrdac et al., 2022). As of today, however, pulse coupling in θ-neurons has widely eluded a biological justification, and the role of the pulse shape for the collective dynamics remained unclear. I hope that the ideas put forward in section 2 contribute to the discussion in a productive way. In particular, I offered two alternative interpretations of pulses. As long as pulses of arbitrary shape are sufficiently narrow, they can reflect swift synaptic transmission including both the pre- and postsynaptic site (see section 2.2). Alternatively, pulses between θ-neurons can describe voltage-gated conductances, or neurotransmitter release, at the presynaptic site (see section 2.3). This second interpretation builds on the change of coordinates through the inverse transform $\theta_j = 2\arctan(v_j)$ from the QIF model (see remark 3), which implicates, however, that the network of pulse-coupled θ-neurons may no longer represent the canonical model for the universal class of weakly connected class 1 excitable neurons.

Pulse-coupling approaches in networks of (quadratic) integrate-and-fire neurons are by default simpler, as synaptic transmission is generally modeled with δ-spikes. Other forms of pulse coupling are rarely found in the literature, although the model formulation in terms of voltages v—as opposed

to the phase description of the θ-neuron—is in principle favorable for modeling voltage-dependent synaptic activation, which may entail pulses $p(v)$ with variable shapes. The shape of the emitted pulse, however, depends not only on the activation function p but also on the action potential. This can become critical for integrate-and-fire neurons because their fire-and-reset mechanism implicates action potentials with a rather artificial shape: at the moment of the spike, the neuron's voltage is instantaneously reset and then starts integrating again (see Figure 1c). A sigmoidal activation function of the presynaptic voltage, similar to those used in conductance-based neurons, then lops off the pulse of an integrate-and-fire neuron right after its spike. The resulting pulse exhibits a moderate increase and a radical decrease much in contrast to those pulses generated by conductance-based neurons (Figures 3 and 4).

Biological concerns aside, networks of heterogeneous QIF neurons with synapses exhibiting such a sigmoidal voltage dependence were studied by Ratas and Pyragas (2016). The synaptic pulses of finite width turned out be a necessary ingredient to synchronize QIF neurons and led to collective oscillations, whereas global coupling via instantaneous δ-spikes is known to rule out collective oscillations of QIF neurons (Montbrió et al., 2015; Jüttner et al., 2021). Yet the voltage-dependent pulses in Ratas and Pyragas (2016) synchronized only excitatory, but not inhibitory, neurons, which is at odds with the theoretical finding that class 1 neurons (including the QIF model) tend to be much more easily synchronized by mutual inhibition than excitation (Wang, 2010). A mechanistic explanation for this paradox has been elusive but may fall back to the artificial shape of the QIF's action potential. The conventional sigmoidal description of voltage-dependent pulses thus had to be revised to compensate for the abrupt fire-and-reset mechanism of QIF neurons and eventually to reveal general principles of emergent collective behavior in spiking neuron networks. In section 2.3, I proposed such a compensation scheme by taking the QIF's action potential into account, which led to a variety of (a)symmetric pulses that unfortunately are analytically intractable to study the network dynamics in more detail. Therefore, I approximated those pulses by analytically more favorable pulses $p_{r,\varphi,\psi}$ in section 2.4, which allowed for exact low-dimensional collective dynamics of globally pulse-coupled QIF neurons (see section 3). As their attractors lie on the invariant Lorentzian manifold, it sufficed to study the RV dynamics, equation 3.6, with the mean pulse activity $P_{r,\varphi,\psi} = \langle p_{r,\varphi,\psi} \rangle$, which are two-dimensional and amenable to a comprehensive bifurcation analysis for instantaneous pulse coupling through $p_{r,\varphi,\psi}$.

I note that in the framework of the RV dynamics, equation 3.6, on the Lorentzian manifold, pulsatile coupling is not restricted to the (smooth) pulses $p_{r,\varphi,\psi}$ proposed above. It is possible to design different voltage-dependent pulses $p(v)$ that allow for an accessible mean field $P(R, V) = \langle p \rangle = \int_{\mathbb{R}} p(v)\mathcal{W}(v, t)dv$ closed in R and V thanks to the averaging with respect to the invariant Cauchy-Lorentz distribution density $\mathcal{W}(v, t)$

of the total voltage density, equation 3.5, of globally coupled QIF neurons. This approach was pursued by Ratas and Pyragas (2016), who used uniform (square) pulses $p_{\mathrm{sq}}(v)$ that are activated when a neuron's voltage exceeds the value $v_{\mathrm{on}} \leq \infty$ and terminated right at the spike time (see equation 4.6) with $v_{\mathrm{off}} = \infty$. By averaging the pulses $p_{\mathrm{sq}}(v)$ with respect to $\mathcal{W}(v,t)$, one obtains the mean presynaptic pulse activity $P_{\mathrm{sq}} = \langle p_{\mathrm{sq}} \rangle$ of the square pulses $p_{\mathrm{sq}}(v)$, equation 4.7, which can readily be used as the recurrent input I_{syn} in the RV dynamics, equation 3.6. Importantly, this approach only applies to the dynamics on the Lorentzian manifold, where the voltages of globally coupled QIF neurons are known to be distributed according to Cauchy-Lorentz distribution density, equation 3.5. To capture transient dynamics beyond the Lorentzian manifold, one has to resort to the exact low-dimensional system, equation 3.4, and the mean pulse activity $\langle p \rangle$ can no longer be found by averaging with respect to $\mathcal{W}(v,t)$, but has to be determined in terms of the macroscopic variables Φ, λ, and σ. This can be achieved, for example, by following the strategy outlined in appendix G. In general, this strategy requires certain assumptions on the pulse functions $p(v)$—which the smooth pulses $p_{r,\varphi,\psi}$ given by 2.10 satisfy but $p_{\mathrm{sq}}(v)$ does not (see, e.g., equation 4 in Ratas & Pyragas, 2019, and compare with appendix F)—but eventually allows for a rigorous and exact mean-field reduction, as well as for the mathematical analysis of the collective dynamics, of pulse-coupled networks of spiking neurons.

5.2 Pulse Parameters, Delays, and Gap Junctions. In this section, I discuss the three parameters—pulse width r, asymmetry φ, and shift ψ—in more detail that shape the smooth pulses $p_{r,\varphi,\psi}$ and, in turn, also the collective dynamics of pulse-coupled neuron networks.

The first parameter $r \in [-1,1]$ tunes the width of the pulse and interpolates between continuous, flat ($r = -1$), and discrete event-triggered ($r = 1$) synaptic transmission. Even for large $0 \ll r < 1$, the pulsatile transmission is smooth, and the presynaptic neuron almost always sends out a signal. Still, the larger is r, the more localized is this signal around a particular (threshold) voltage $v \approx v_{\mathrm{thr}} = \tan(\psi/2)$ or, equivalently, a particular central phase $\theta \approx \psi$. The effect of the emitted pulse (with large r) on the postsynaptic neuron becomes negligible for voltages farther away from v_{thr} (see Figure 7a, right panel). If v_{thr} coincides with the QIF spiking threshold v_p at infinity ($v_{\mathrm{thr}} = v_p \to \infty$), and in absence of asymmetry ($\varphi = 0$), the rectified-Poisson (RP) pulses $p_{r,0,\pi}$ resemble the Ariaratnam-Strogatz (AS) pulses $p_{\mathrm{AS},n}$ that have been frequently employed in the context of θ-neuron networks (see, e.g., Goel & Ermentrout, 2002; Ermentrout, 2006; Luke et al., 2013, 2014; So et al., 2014; Laing, 2014, 2015, 2016a, 2016b, 2018a, 2018b; Roulet & Mindlin, 2016; Laing, 2017; Chandra et al., 2017; Aguiar et al., 2019; Lin et al., 2020; Laing & Bläsche, 2020; Laing & Omel'chenko, 2020; Means et al., 2020; Bläsche et al., 2020; Bick et al., 2020; Jüttner et al., 2021; Omel'chenko & Laing, 2022; Bîrdac et al., 2022). The usability of AS pulses,

however, is hampered by the series representation of the mean pulse activity $\langle p_{\mathrm{AS},n}\rangle$. The larger is n, the narrower the AS pulse, and the more convoluted $\langle p_{\mathrm{AS},n}\rangle$ (see appendix E). In fact, $\langle p_{\mathrm{AS},n}\rangle$ does not allow for a closed-form description in the exact low-dimensional system, equation 3.4. By contrast, the mean RP pulse activity $P_{\mathrm{RP},r} = \langle p_{r,0,\pi}\rangle$ can be expressed in terms of the three macroscopic variables Φ, λ, σ that completely determine the collective dynamics. On the Lorentzian manifold, $P_{\mathrm{RP},r}$ simplifies to a concise function of the firing rate R and the mean voltage V (see equation 3.9) and allows for a straightforward bifurcation analysis even for arbitrarily narrow pulses (see section 4.2).

The second parameter, $\psi \in [0, 2\pi)$, shifts the pulse to the right ($\psi > \pi$) or to the left ($\psi < \pi$), but does not change its actual shape. For symmetric pulses ($\varphi = 0$), the pulse is strongest at the phase $\theta = \psi$, or when the presynaptic voltage v crosses the virtual threshold $v_{\mathrm{thr}} = \tan(\psi/2)$. The nomenclature of a virtual threshold becomes rigorous for Dirac δ-pulses $p_{1,0,2\arctan(v_{\mathrm{thr}})}$, that are emitted at the moment when $v = v_{\mathrm{thr}}$. Depending on the sign of v_{thr}, the pulse is shifted to the right or to the left of the QIF spiking threshold $v_p = \infty$, which can be interpreted as an effective delay or advance of the postsynaptic response (see Ermentrout, 1996; Gutkin et al., 2001). Indeed, if the pulse reaches its peak when $v = v_{\mathrm{thr}} \ll 0$, then the effect on the postsynaptic response is strongest after the actual spiking of the presynaptic neuron. On the other hand, for $v_{\mathrm{thr}} \gg 0$, the emitted pulse is strongest before the neuron has spiked.

For threshold values after the spike, $v_{\mathrm{thr}} < 0$, and as expected for delayed synaptic transmission (Roxin et al., 2005; Roxin & Montbrió, 2011), collective oscillations can be found for inhibition ($J < 0$) and (strong) excitatory drive $I_0 > 0$ (see Figures 8b and 8c). The results are qualitatively identical for sufficiently narrow pulses with width $0 \ll r \leq 1$ and threshold value $v_{\mathrm{thr}} \ll 0$, so that it suffices to report the phase diagram for one set of parameters only (here, $r = 0.95$, $v_{\mathrm{thr}} = -20$). As a word of caution, I stress that shifted pulses mimic truly delayed pulses only on the single neuron level; on the macroscopic level, they may lead to very distinct collective dynamics. Reminiscent of that is the cusp-shaped region of bistability between two (very) low-activity states for $J < 0$ in Figures 8b and 8c. Note also that in contrast to "real" time delays, instantaneous recurrent coupling with shifted pulses cannot store the neurons' history and transmit it unaltered after the delay. That is why the RV dynamics, equation 3.6, remain low-dimensional, whereas real delays yield infinite-dimensional dynamics that can entail more complex collective behavior (Pazó & Montbrió, 2016; Devalle et al., 2018).

For advanced (or left-shifted) pulses with threshold values before the spike ($0 \ll v_{\mathrm{thr}} < \infty$), collective oscillations occur for excitatory coupling ($J > 0$) and cease via a supercritical Hopf bifurcation when decreasing the coupling strength (see Figure 9 and equation 4.5). This insight also explains why the square pulses, equation 4.6, used by Ratas and Pyragas (2016),

whose mean is shifted to the phase before the actual spike, induce collective oscillations only for excitatory neurons but not in the biologically more plausible case of inhibition (see section 4.4 and 5.1). Moreover, the observed bifurcation scenario for left-shifted pulses resembles the case of gap junction-coupling (see Figure 7 of Pietras et al., 2019). Gap junctions are, in general, known to promote neural synchrony and facilitate collective oscillations (Laing, 2015; Pietras et al., 2019). QIF neurons that are globally coupled via gap junctions of strength J (but not via pulses) have the subthreshold dynamics

$$\tau_m \dot{v}_j = v_j^2 + i_0 + \frac{J}{N}\sum_{k=1}^{N}(v_k - v_j) + I_j. \tag{5.2}$$

On the Lorentzian manifold, the exact RV dynamics corresponding to the microscopic dynamics, equation 5.2, in the limit $N \to \infty$ takes on the same form as equation 3.6 when identifying $V = \langle v_j \rangle - J/2$ as a shifted mean voltage, $I_0 = i_0 + J^2/4$ and recurrent synaptic input $I_{\text{syn}} = JV$. Thus, in line with the results of section 4.1, the onset of collective oscillations in the gap junction coupled network, equation 5.2, is neatly explained by an effective voltage coupling. The similarity between the collective dynamics for advanced pulses on one hand and for gap junctions on the other hand supports the notion that pulse interactions indeed induce an effective voltage component in the recurrent coupling. Again a word of caution is due about the correct interpretation of temporally versus effectively advanced pulses: with instantaneous pulse coupling, the mean field $\langle p_{r,0,2\arctan(v_{\text{thr}})} \rangle$ has an immediate effect on individual neurons. That is, emitting an inhibitory pulse before the actual spike may possibly hinder the same neuron to actually spike. By allowing for synaptic kinetics, as in equations 5.4 or 5.5 below, one can alleviate this intricacy and indeed interpret the time at which a neuron crosses the virtual threshold v_{thr} as the activation time t_a of the postsynaptic response (see Ermentrout, 1996).

Finally, the asymmetry parameter $\varphi \in [-\pi, \pi)$ skews the pulse $p_{r,\varphi,\psi}(\theta)$ and shifts its bulk to the right ($\varphi > 0$) or to the left ($\varphi < 0$) of the central phase $\theta = \psi$; note that $\varphi \neq 0$ is only effective for pulses of finite width $r < 1$. Already a small value of $0 < |\varphi| \ll 1$ can have a large effect on the network dynamics and easily induce collective oscillations (see Figures 6b and 8d). If the pulses are slightly skewed to the phase after the spike ($\varphi > 0$), collective oscillations emerge almost naturally for inhibition ($J < 0$) with sufficient excitatory drive ($I_0 > 0$). The effect is similar to that of synaptic kinetics and, indeed, for these right-skewed pulses, one retrieves a fast rise and slower decay of the postsynaptic response (see Figure 4c2) as observed for first- and second-order synapses. For left-skewed pulses ($\varphi < 0$), by contrast, the mean of the pulse is advanced, and collective oscillations emerge only for excitation ($J > 0$; see Figure 9), similar to left-shifted pulses ($\psi < \pi$, $v_{\text{thr}} > 0$) or gap junctions.

5.3 Can Instantaneous Pulses Replace Complex Synaptic Transmission? In contrast to the mathematical abstraction of δ-spikes, smooth pulses of finite width have often been assumed to be biologically more realistic and to better approximate postsynaptic responses like those of conductance-based, Hodgkin-Huxley-like neuron models (Ermentrout, 2006; Luke et al., 2013; Bick et al., 2020). It seems daunting to include various levels of biochemical realism at a chemical synapse, so in general one jumps over the explicit modeling of (1) how an increase (depolarization) in the voltage v_{pre} of a presynaptic neuron activates voltage-gated Ca^{2+} channels, (2) how the Ca^{2+}-influx induces the release of neurotransmitters that diffuse to the postsynaptic neuron and bind to specific receptors with different possible mechanisms (Kaeser & Regehr, 2014), and (3) how the binding of neurotransmitters triggers the opening of ionic channels and eventually generates a postsynaptic current. Instead, the synaptic process is described phenomenologically—but not derived from first principles (Koch, 2004)—by the synaptic input I_{syn} to the postsynaptic neuron,

$$I_{\text{syn}} = -g_{\text{syn}}\big(v_{\text{pre}}(t), t\big)\big[v_{\text{post}}(t) - E_{\text{syn}}\big], \tag{5.3}$$

with reversal potential E_{syn} and a synaptic conductance that is often represented as $g_{\text{syn}}(t) = \hat{g}_{\text{syn}} s(t)$ with maximal synaptic conductance $\hat{g}_{\text{syn}} \geq 0$ and a gating variable $s(t)$ that may be interpreted as the fraction of open channels releasing neurotransmitters. If the synaptic conductance is activated by a (sigmoidal-like) function $f(v_{\text{pre}})$ of the presynaptic membrane potential, as discussed in section 2.3, and follows first-order synaptic kinetics, the dynamics of the gating variable $s(t)$ is given by

$$\dot{s} = a_r f\big(v_{\text{pre}}(t - \tau_l)\big)(1 - s) - a_d s. \tag{5.4}$$

The constants a_r and a_d determine the rise and decay times of the postsynaptic response (Wang & Rinzel, 1992; Wang & Buzsáki, 1996; Destexhe et al., 1994; Ermentrout & Terman, 2010), and a possible latency time τ_l can account for finite axonal propagation times (Ermentrout & Terman, 2010). Depending on the shape of the presynaptic action potential, $s(t)$ can actually begin to rise before the presynaptic voltage reaches its peak (corresponding to the neuron's spike time T_{pre}), especially when the action potential is broad (Ermentrout, 1996). Alternatively to equation 5.4, the time course of $s(t)$ can be described by the difference of two exponential functions,

$$s(t) = A\big[e^{-(t-t_a)/\tau_r} - e^{-(t-t_a)/\tau_d}\big],\ t \geq t_a, \tag{5.5}$$

with amplitude A and activation time t_a, which is typically around the spike time T_{pre} of the presynaptic neuron plus some latency τ_l (possibly due to finite axonal propagation speed and taking into account that the

postsynaptic response may start before T_{pre}). Biexponential synapses (see equation 5.5) with characteristic latency, rise, and decay time constants $\tau_{l,r,d}$ are the gold standard in computational models of spiking neurons—they allow for mean-field approaches (Treves, 1993; Abbott & van Vreeswijk, 1993; Brunel & Hakim, 1999; Brunel & Wang, 2003; Brunel & Hansel, 2006) and are typically reported in the experimental neuroscience literature (although there are no coherent definitions for $\tau_{l,r,d}$).

In network models of spiking QIF or θ-neurons, pulses $p_{r,\varphi,\psi}$ of finite width ($r < 1$), as described by equation 2.10, are an ideal candidate for the presynaptic voltage-dependent activation, or release, function $f(v_{\text{pre}})$ in equation 5.4. The pulse is activated shortly before the QIF neuron reaches the peak of its action potential (see Figure 4) and can last even through its recovery period (see section 2.3). The versatility of the pulses $p_{r,\varphi,\psi}$ further allows accentuating the synaptic activation, or the release of neurotransmitters, on either phase of the action potential through the asymmetry parameter $\varphi \neq 0$ or the shift parameter $\psi \neq \pi$. Thereby, it is possible to account for physiological conditions under which the opening of voltage-gated Ca^{2+} channels, and consequently neurotransmitter release, is advanced, for example, at an increased temperature (Sabatini & Regehr, 1996, 1999; Volgushev et al., 2004; Yang & Wang, 2006; Chao & Yang, 2019; Van Hook, 2020).

When including synaptic kinetics of the form 5.4 that are activated by voltage-dependent pulses, one has to be careful how to incorporate the corresponding postsynaptic responses in mean-field models. Indeed, when summing over a large number of postsynaptic responses s_j, the product $f(v_{\text{pre,j}})(1 - s_j)$ with the presynaptic pulses $f(v_{\text{pre,j}})$ presents a nonlinear problem that can only be resolved approximately,[7] even for the analytically tractable pulses $f(v_{\text{pre,j}}) = p_{r,\varphi,\psi}(\theta_j)$. Biexponential synapses (see equation 5.5) do not suffer from this shortcoming, which may explain their success in (mean-field models in) computational neuroscience. As the postsynaptic response s_j is typically activated at the presynaptic spike time T_j, it is advantageous to rewrite equation 5.5 as

$$\tau_d \dot{s}_j = -s_j + u_j, \;\; \tau_r \dot{u}_j = -u_j + \tau_0 p_{1,0,\pi}\big(\theta_j(t - \tau_l)\big), \tag{5.6}$$

[7] When summing the responses s_j over all presynaptic neurons j with individual responses given by equation 5.4, the mean response reads $\dot{S} = \langle \dot{s}_j \rangle = a_r \langle p_{r,\varphi,\psi} \rangle - a_d S - a_r \langle p_{r,\varphi,\psi}(\theta_j) s_j \rangle$. The last term $\langle p_{r,\varphi,\psi}(\theta_j) s_j \rangle$ represents an average of the product of the presynaptic pulse with the current state of the postsynaptic response. In general, $p_{r,\varphi,\psi}(\theta_j)$ and s_j are not independent but correlated, so that taking the mean of their product does not yield a closed equation in terms of S and $\langle p_{r,\varphi,\psi} \rangle$. For δ-spikes (in the limit $(r, \varphi, \psi) \to (1, 0, \pi)$) and under the Poissonian assumption that presynaptic spike trains have a coefficient of variation (CV) close to 1, one can approximate $\langle p_{1,0,\pi}(\theta_j) s_j \rangle \approx (\pi \tau_m R) S$ (see Pietras et al., 2022), and possibly loosen the Dirac δ-pulse assumption to obtain $\langle p_{r,\varphi,\psi}(\theta_j) s_j \rangle \approx \langle p_{r,\varphi,\psi} \rangle S$ for r close to 1. Yet the Poissonian assumption, and hence the foregoing approximation, is difficult to justify in strongly correlated collective states, for example, of regular synchrony (Clusella & Montbrió, 2022).

with normalization factor τ_0; one retrieves equation 5.5 for $\tau_0 = A(\tau_d - \tau_r)/(2\pi\tau_r\tau_d)$. To avoid infinite-dimensional time-delayed neuronal dynamics when $\tau_l > 0$, one can follow Ermentrout (1996) and use shifted Dirac δ-pulses $p_{1,0,2\arctan(v_{\text{thr}})}$ with a negative virtual threshold $v_{\text{thr}} < 0$ that effectively delay the postsynaptic response. Likewise, one can use positive virtual thresholds $v_{\text{thr}} > 0$ to account for activation times of the synapse before the actual spike time, $t_a < T_j$. Since there are no nonlinear terms in equation 5.6, one can readily average the postsynaptic responses over the population and obtain a concise mean-field model.

While I have shown how to interpret, and incorporate, the novel pulse function $p_{r,\varphi,\psi}(\theta)$ in the traditional framework of synaptic transmission, one question remains: Are instantaneous pulses of finite width adequate for replacing the complex processes involved in generating a postsynaptic current $I_{\text{syn}}(t)$ of the form 5.3? In other words, can instantaneous pulses $p_{r,\varphi,\psi}$ approximate (the effect of) $I_{\text{syn}}(t)$ sufficiently well as previously hypothesized? To answer this question, I decompose the problem into two parts because I_{syn} comprises two distinct mechanisms: *synaptic kinetics* (encoded in the dynamics of s) and *conductance-based synapses* (due to the explicit voltage-dependence in $[E_{\text{syn}} - v_{\text{post}}(t)]$). As I will argue, instantaneous pulses of finite width are not suited to replace either synaptic kinetics (see section 5.3.1) or conductance-based synapses (see section 5.3.2) in networks of QIF or θ-neurons, but should rather be used complementary to traditional synaptic transmission (see section 5.3.3).

5.3.1 Pulses of Finite Width Do Not Replace Synaptic Kinetics. To focus on the effect of synaptic kinetics, it is convenient to approximate the term $E_{\text{syn}} - v_{\text{post}}(t) \approx v_{\text{eff}}$ in equation 5.3 by an effective potential v_{eff}. This approximation is valid if $v(t)$ spends most of the time near its rest state, and the recurrent synaptic input I_{syn} in the QIF dynamics, equation 3.1, is given by $I_{\text{syn}}(t) = JS(t)$ with $J = \hat{g}_{\text{syn}} v_{\text{eff}}$ and $S(t) = \langle s_j(t) \rangle$. Depending on the sign of v_{eff}, the coupling J is excitatory ($v_{\text{eff}} > 0$) or inhibitory ($v_{\text{eff}} < 0$). The question is now whether the time course of $s_k(t)$ as a postsynaptic response to the spiking of presynaptic neuron k can be equally well explained with an instantaneous pulse $s_k(t) = p_{r,\varphi,\psi}(\theta_k(t))$ or with a δ-spike-triggered biexponential synapse, equation 5.5, with realistic latency, rise, and decay time constants.

For simplicity, I consider two inhibitory QIF neurons coupled via shifted pulses $p_{r,0,\psi}$ of finite width $r = 0.95$ (see Figure 8a, blue curve). The membrane time constant is fixed at $\tau_m = 10$ ms. Neuron 1 receives a constant input $I_1 = 0.5$ and spikes at frequency $100/(\sqrt{2}\pi) \approx 22.5$ Hz, whereas neuron 2 receives $I_2 = -1$ and remains quiescent at its resting potential, $v_{2,\text{rest}} = -1$. The shift parameter ψ is chosen such that the pulse is strongest when the voltage v of the presynaptic neuron crosses the virtual threshold $v_{\text{thr}} = -20 = \tan(\psi/2)$ after recovering from its reset. In this example, a pulse emitted by neuron 1 is strongest approximately 0.5 ms after its

spike and the postsynaptic current of neuron 2 is proportional to $s_1(t) = p_{0.95,0,-2\arctan 20}(\theta_1(t))$. The postsynaptic potential (PSP) $v_2(t)$ evolves according to $\tau_m \dot{v}_2 = v_2^2 - 1 + Js_1(t)$ with $J = -\pi$ and exhibits a rapid rise and more moderate decay with its peak at approximately 1.08 ms after the presynaptic spike. One can fit the voltage response $v_2(t)$ of neuron 2 to that produced by a biexponential synapse, equation 5.5, activated at the time of the presynaptic spike at $t = 0$ with $\tau_l = 0$ ms. The agreement between the voltage responses (PSPs) to the instantaneous pulse and to the biexponential synapse is remarkable, even though the perceived PSCs are quite different (see Figure 10a). Nonetheless, the fitted rise and decay times, $\tau_r = 0.025$ ms and $\tau_d = 0.55$ ms, are by far shorter than those reported in the literature (e.g., $\tau_r = 0.5$ ms and $\tau_d = 5$ ms used by Wang & Buzsáki, 1996 and Brunel & Wang, 2003). Furthermore, the duration from the presynaptic spike until the peak of the PSP differ by 0.2 ms (peak pulse response at 1.08 ms versus peak synaptic response at 1.28 ms). This calls for introducing a latency time constant of $\tau_l = 0.2$ ms, which seems a reasonable value. For wide pulses ($r = 0.75$), however, the fitted latency increases and the postsynaptic response will be prompted at very low presynaptic voltage thresholds $v_{\text{thr}} \approx 0$ long before the actual spiking threshold.

Besides unrealistic synaptic time constants, another shortcoming of instantaneous pulses is the impossibility of integrating rapidly incoming inputs. While this is not a problem for very fast synaptic kinetics (with short rise and decay time constants $\tau_{r,d}$), synaptic integration becomes important for realistic synaptic decay of around $\tau_d = 5$ ms. In the context of the two neurons from before, increasing the input of neuron 1 to $I_1 = 50$ induces spiking at a faster frequency of $100\sqrt{50}/\pi \approx 225$ Hz. In the case of synaptic kinetics, the postsynaptic neuron 2 integrates the subsequent spikes from neuron 1 and both PSC and PSP exhibit increased baseline levels. The inhibitory effect on the postsynaptic voltage v_2 is thus significantly larger as compared to instantaneously transmitted pulses of finite width (see Figure 10b).

In sum, instantaneous pulses of finite width can have a similar effect on individual postsynaptic voltage responses as biexponential synapses, but the comparison is misleading. First, the fitted time constants of biexponential synapses are far from realistic, and, second, instantaneous pulses cannot integrate inputs, an important hallmark of synaptic kinetics. Hence, instantaneous pulses $p_{r,\varphi,\psi}$ do not replace synaptic kinetics.

5.3.2 Pulses Do Not Describe Conductance-Based Synapses. Can instantaneous pulses of finite width substitute for conductance-based synapses? To study the additional voltage-dependence in equation 5.3, I focus on instantaneous conductance-based synapses, that is, $g_{\text{syn}}(t) = (\hat{g}_{\text{syn}}/N)\sum_k \delta(t - T_k^l)$ is proportional to the spike train of the presynaptic neurons. The voltage dynamics, equation 3.1, of globally coupled QIF neurons then becomes

$$\tau_m \dot{v}_j = v_j^2 + I_0 - \hat{g}_{\text{syn}} \tau_m R(t)[v_j - E_{\text{syn}}] + I_j(t) \tag{5.7}$$

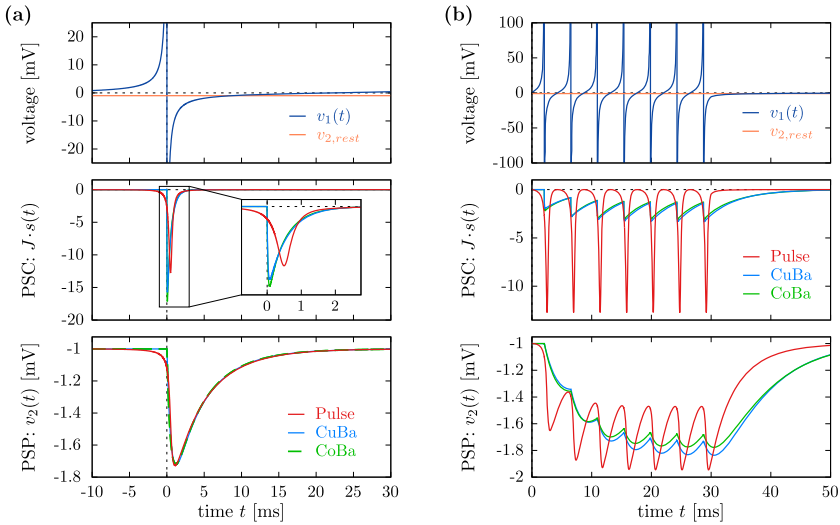

Figure 10: Pulse coupling (red) does not replace traditional synaptic transmission via current-based (CuBa, blue) or conductance-based (CoBa, green) synapses with synaptic kinetics. Top: Presynaptic voltage traces v_j of periodically spiking neuron $j = 1$ (blue) and excitable neuron $j = 2$ with constant input $I_2 = -1$ and resting potential $v_{2,\text{rest}} = -1$ (orange). Middle: Postsynaptic currents elicited by presynaptic neuron 1 according to a pulse $Jp_{0.95,0,-2\arctan(20)}(\theta_1)$, CuBa synapse $Js_1(t)$, or CoBa synapse $\hat{g}_{\text{syn}} s_1(t)[E_{\text{syn}} - v_2(t)]$, where $s_1(t)$ follows equation 5.6 with $\tau_0 = 1$, $\tau_l = 0$. For the inhibitory synapse, $J = -\pi$ and $\hat{g}_{\text{syn}} = 1.12\pi/4$ are chosen such that the PSPs (bottom) almost coincide; $E_{\text{syn}} = -5$ and $\hat{g}_{\text{syn}} v_{\text{eff}} \approx J$ with $v_{\text{eff}} = (E_{\text{syn}} - v_{2,\text{rest}}) = -4$. Bottom: Postsynaptic potential/voltage response $v_2(t)$ according to PSCs. (a) The voltage trace $v_2(t)$ in response to a single spike ($I_1 = 0.5$) can be sufficiently well described by pulses and more complex synaptic dynamics with short synaptic time constants $\tau_r = 0.025$ ms and $\tau_d = 0.55$ ms. (b) Synaptic integration of rapidly incoming spikes ($I_1(t) = 50$ for $t \leq 30$ ms and 0 afterward) is characteristic for CuBa and CoBa synapses with realistic decay $\tau_d = 5$ ms, but not feasible with instantaneous pulses $p_{r,\varphi,\psi}$.

with I_j as in equation 3.1b and the same fire-and-reset rule at infinity as before. For positive maximal synaptic conductance $\hat{g}_{\text{syn}} > 0$, the reversal potential E_{syn} determines whether the (net effect of the) recurrent coupling is excitatory ($E_{\text{syn}} > 0$) or inhibitory ($E_{\text{syn}} < 0$).

As in section 5.3.1 about synaptic kinetics, one can compare the postsynaptic voltage response to a presynaptic periodically spiking neuron when the neurons interact via (δ-spike-activated) conductance-based synapses or via (instantaneous) pulses of finite width. With $I_{1,2}$ as before and setting $\hat{g}_{\text{syn}}(E_{\text{syn}} - v_{\text{rest}}) = J$ with $v_{\text{rest}} = -\sqrt{-I_2} = -1$, the PSC for the conductance-based synapse, equation 5.7, is identical to a δ-spike of strength J, and

the voltage responses can only be approximated by sufficiently narrow pulses $p_{r,\varphi,\pi}$ with $r \to 1$. When augmenting the conductance-based synapse equation 5.7, by second-order synaptic kinetics, that is, $R(t)$ in equation 5.7, is replaced by $s_j(t)$ according to equation 5.6, the resulting postsynaptic response almost coincides with the one by the biexponential synapse (see Figure 10). Therefore, the pulse approximation of the second-order conductance-based synapse suffers from the same shortcomings—unrealistic synaptic time constants and impossibility of synaptic integration—as is the case for the biexponential synapse.

On top of that, the pulse approximation of conductance-based synapses becomes problematic in networks of (heterogeneous) QIF neurons even though the PSP amplitude of an individual neuron receiving conductance-based synaptic input matches the PSP for narrow pulse coupling (see Figure 10). But when a group of neurons receive heterogeneous inputs, they have variable resting potentials, and, consequently, the resulting PSP amplitudes differ across the network. The PSPs may even vary in time as they depend on the current state of each neuron. This feature of neural networks with conductance-based synapses is hardly possible to implement by pulses with a predefined shape that is, moreover, common to all neurons.

In addition, there are significant differences between instantaneous pulse coupling and conductance-based synapses with respect to the collective dynamics. As shown in section 4, instantaneous pulses of finite width generate, in general, collective oscillations in large networks of QIF neurons (albeit the parameter regions for symmetric pulses may seem degenerate). By contrast, globally coupled QIF neurons with instantaneous conductance-based synapses, equation 5.7, do not support collective oscillations that emerge via a Hopf bifurcation from an asynchronous state. The proof follows the same lines as in section 4.1. On the Lorentzian manifold, the RV dynamics equation 3.6, for the microscopic dynamics, equation 5.7, are

$$\tau_m \dot{R} = \frac{\gamma}{\pi \tau_m} + 2RV - \hat{g}_{\mathrm{syn}} \tau_m R^2, \tag{5.8a}$$

$$\tau_m \dot{V} = V^2 - (\pi \tau_m R)^2 + \hat{g}_{\mathrm{syn}} \tau_m R[E_{\mathrm{syn}} - V] + I_0. \tag{5.8b}$$

The fixed-point solutions (R^*, V^*) of equation 5.8 satisfy $V^* = \hat{g}_{\mathrm{syn}} \tau_m R^*/2 - \gamma/(2\pi \tau_m R^*)$. A necessary condition for the oscillatory instability of (R^*, V^*) via a Hopf bifurcation is that the trace of the Jacobian $\mathrm{Jac}_{\mathrm{CoBa}}$ of equation 5.8 vanishes. Here, however,

$$\mathrm{tr}(\mathrm{Jac}_{\mathrm{CoBa}}) = -\frac{2\gamma}{\pi \tau_m R^*} - \hat{g}_{\mathrm{syn}} \tau_m R^* < 0$$

is always negative because $\gamma, \hat{g}_{\mathrm{syn}}, \tau_m R^* > 0$ by definition. Hence, collective oscillations never occur through a Hopf bifurcation in networks of globally

coupled QIF neurons with instantaneous conductance-based synapses that are triggered by presynaptic spikes. In conclusion, pulses of finite width do not account for conductance-based synapses, either.

5.3.3 Pulse-Triggered Synaptic Kinetics. Synaptic kinetics need not be triggered by δ-spikes but can also be initiated by general pulses $p_{r,\varphi,\psi}$, which can be thought of as a combination of equations 5.4 and 5.6. Replacing the δ-spikes in equation 5.6 by general pulses $p_{r,\varphi,\psi}$, leads to the microscopic synaptic dynamics

$$\tau_d \dot{s}_j = -s_j + u_j, \quad \tau_r \dot{u}_j = -u_j + p_{r,\varphi,\psi}\big(\theta_j(t)\big). \tag{5.9}$$

The response dynamics, equation 5.9, triggered by a narrow and possibly asymmetric pulse is more general than the conventional δ-spike-triggered biexponential synapse, equation 5.5. First, it connects the response with the presynaptic action potential in a continuous manner and thereby avoids the open discussion at which instant the synaptic response is actually triggered: Does the activation time t_a in equation 5.5 denote the peak voltage of the action potential or a seemingly arbitrary threshold value? And second, the pulse-triggered second-order dynamics, equation 5.9, can be used to fit more complex, experimentally verified impulse responses, for example, for hippocampal neurons with an impulse response given by a multiexponential function (Bekkers & Stevens, 1996),

$$s(t) = s_{\max}\{1 - \exp[-(t - t_a)/\tau_r]\}^x \exp[-(t - t_a)/\tau_d],$$

or, in the realm of biomechanics, for motor-unit twitches upon motoneuron discharge, whose impulse response is given by a generalized alpha function (Fuglevand et al., 1993; Raikova & Aladjov, 2002; Contessa & Luca, 2013),

$$s(t) = s_{\max}(t - t_a)^x \exp[-(t - t_a)/\tau_d].$$

In both cases, x is a real-valued parameter (and not an integer), so that the dynamics of $s(t)$ cannot be described with (analytically tractable) differential equations.

On the network level, pulse-triggered synaptic kinetics, equation 5.9, further permit a concise mean-field reduction of the collective dynamics as before. For global coupling of strength J, the recurrent synaptic input is given by $I_{\text{syn}} = JS(t)$ with $S(t) = \langle s_j(t)\rangle$. As I set $\tau_0 = 1$ and $\tau_l = 0$ in equation 5.6 to obtain equation 5.9, I have ensured that the macroscopic fixed points satisfy $S^* = P_{r,\varphi,\psi}(R^*, V^*)$, which allows for a direct comparison with instantaneous synaptic transmission in the limit $\tau_r = \tau_d \to 0$ (see Figure 8d) for an example; a comprehensive comparison, however, is beyond the scope of this article. The exact, augmented RV dynamics of globally coupled QIF neurons

with second-order synaptic kinetics, equation 5.9, read on the Lorentzian manifold,

$$\tau_m \dot{R} = \frac{\gamma}{\pi \tau_m} + 2RV, \tag{5.10a}$$

$$\tau_m \dot{V} = V^2 - (\pi \tau_m R)^2 + I_0 + JS(t), \tag{5.10b}$$

$$\tau_d \dot{S} = -S + U, \tag{5.10c}$$

$$\tau_r \dot{U} = -U + P_{r,\varphi,\psi}(R, V), \tag{5.10d}$$

with the mean presynaptic activity $P_{r,\varphi,\psi}$ fully determined in terms of R and V according to equation 3.8. For instantaneous rise time $\tau_r \to 0$, equation 5.10 describes the RV dynamics with first-order synaptic kinetics (with exponential decay τ_d). For $\tau_r = \tau_d$, the second-order synaptic kinetics of the RV dynamics, equation 5.10, reduces to that of the so-called alpha synapse.

For completeness, I also present the pulse-triggered conductance-based RV dynamics with synaptic kinetics by combining equations 5.8 to 5.10:

$$\tau_m \dot{R} = \frac{\gamma}{\pi \tau_m} + 2RV - \hat{g}_{\text{syn}} RS, \tag{5.11a}$$

$$\tau_m \dot{V} = V^2 - (\pi \tau_m R)^2 + \hat{g}_{\text{syn}} S\big[E_{\text{syn}} - V\big] + I_0, \tag{5.11b}$$

$$\tau_d \dot{S} = -S + U, \tag{5.11c}$$

$$\tau_r \dot{U} = -U + P_{r,\varphi,\psi}(R, V); \tag{5.11d}$$

similar conductance-based RV dynamics were reported by Ratas and Pyragas (2016), but with a synaptic variable $S(t)$ for nonsmooth pulses and first-order synaptic kinetics ($\tau_r = 0$); see also the works by Byrne et al. (2017), Coombes and Byrne (2019), Keeley et al. (2019), and Byrne et al. (2020, 2022). Preliminary results suggest that the additional synaptic kinetics in the augmented RV dynamics, equation 5.10 or 5.11, blur the effect of the pulse shape $p_{r,\varphi,\psi}$ on the collective dynamics, especially if the pulse is narrow (see Figure 11). It may hence suffice to resort to the conventional δ-spike-interactions, setting $(r, \varphi, \psi) \to (1, 0, \pi)$, when also studying synaptic kinetics. A comprehensive analysis of the augmented RV dynamics, equations 5.10 and 5.11, shall clarify this hypothesis, which I leave for future work.

6 Conclusions and Outlook

Spiking neural networks are well established in the neurosciences and a powerful tool in understanding cortical information processing, which originates from the exchange of action potentials between neurons. For computational advantages, mathematical tractability, and rigorous

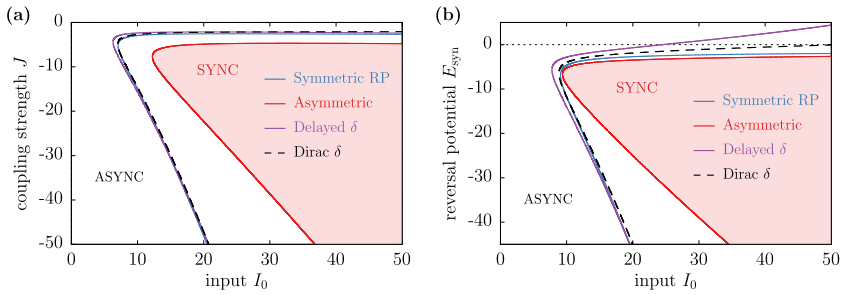

Figure 11: Collective oscillations among inhibitory QIF neurons due to first-order synaptic kinetics of (a) current-based and (b) conductance-based synapses are affected little by the pulse shape $p_{r,\varphi,\psi}$. The Hopf bifurcation boundaries of RP pulses ($r = 0.95$, $\varphi = 0$, $\psi = \pi$; blue) and of delayed δ-pulses ($r = 1$, $\varphi = 0$, $\psi = 2\arctan(-20)$; violet) coincide almost perfectly with the one for δ-spikes ($r = 1$, $\varphi = 0$, $\psi = \pi$; black dashed); for asymmetric pulses ($r = 0.95$, $\varphi = \pi/12$, $\psi = \pi$; red) the Hopf curve is slightly shifted to the right. Collective oscillations are found in the SYNC region to the right of the Hopf boundaries (the shaded region indicates collective oscillations for the red asymmetric pulses). The Hopf boundaries are supercritical and were detected from equations 5.10 and 5.11 with $\tau_m = 2\tau_d = 10$ ms and $\tau_r = 0$. Note that the y-axis in panel b denotes the reversal potential E_{syn} of conductance-based synapses with maximal synaptic conductance $\hat{g}_{\text{syn}} = 1$; E_{syn} plays a remarkably similar role as the coupling strength J for current-based synapses in panel a.

analysis, these networks use simple spiking neuron models that replicate the essential features of real neural dynamics, while interactions between neurons are modeled with infinitely narrow pulses when the presynaptic neuron spikes; these pulses, however, do not capture the more complex dynamics of real synapses. Nonetheless and in support of the spike assumption, recent studies have led to the belief that the shape of the action potential is indeed dispensable on both an individual and a network level: (generalized leaky) integrate-and-fire (GLIF) models, which do not provide access to (realistic) action potentials, were shown to preserve intrinsic properties of single neurons and characteristic features of their spike generation observed in experiments (Mensi et al., 2012; Pozzorini et al., 2015; Teeter et al., 2018). Moreover, GLIF point neurons capture experimentally observed population activity as faithfully as multi-compartment Hodgkin-Huxley-like models do (Rössert et al., 2017; Arkhipov et al., 2018; Billeh et al., 2020). It may be true that the shape of the action potential hardly affects the network dynamics, at least for uncoupled neurons. But as soon as neurons are synaptically connected, the spotlight turns on the action potential. The shape of pulsatile synaptic transmission between neurons directly depends on the action potential and can, ultimately and critically, affect the

network dynamics. By taking the shape of these interactions explicitly into account, the modeling framework proposed here enables a new perspective on pulse shape and voltage-dependent synchronization of spiking neuron networks, which has remained concealed for δ-spike-interactions.

In the first part of this article, I proposed two biologically plausible interpretations of smooth pulsatile synaptic transmission in networks of spiking QIF and θ-neurons; the difference between the two interpretations is subtle and based on the respective modeling assumptions. In general, pulses represent the interplay of a presynaptic action potential with a synaptic activation function p. For QIF and θ-neuron models, p needs to be modified to account for their simplified spiking behavior. When pulse-coupled networks of θ-neurons are meant to replicate (weakly) connected class 1 excitable neurons, the pulses must be sufficiently narrow as they reflect an (almost) instantaneous synaptic transmission process that can include both the presynaptic and the postsynaptic site; this interpretation carries over to QIF neurons (with infinite reset and threshold values) through the forward transformation $v = \tan(\theta/2)$. Alternatively, and not necessarily on the premise that the neurons are class 1 and weakly connected, QIF neurons emit pulses of arbitrary shape that can describe voltage-gated conductances, or the release of neurotransmitters, at the presynaptic site; this interpretation carries over to θ-neurons via the inverse transformation $\theta = 2\arctan v$. In either case, pulses may eventually be interpreted as a continuous generalization of the conventionally used δ-spikes to install neurotransmitter-based chemical synapses.

In the second part, I put forward an exact low-dimensional macroscopic description for large networks of globally coupled QIF or θ-neurons interacting via smooth pulses of various shapes that approximate the previously justified pulses. The modeling framework allows for incorporating the recurrent synaptic input, mediated by a general family of pulse functions $p_{r,\varphi,\psi}$, in terms of a few macroscopic variables. Thereby, one obtains system 3.4 of three complex-valued ordinary differential equations that exactly describes the collective dynamics in the thermodynamic limit. In the presence of (independent Cauchy white) noise or (Cauchy-Lorentz distributed) heterogeneity, the collective dynamics converges to an invariant manifold (Pietras et al., 2023), the so-called Lorentzian manifold (Montbrió et al., 2015), on which the recurrent synaptic input is fully determined by the population firing rate R and the mean voltage V. On this manifold, the firing rate and voltage dynamics—the RV dynamics, equation 3.6—are closed in R and V, remain two-dimensional for instantaneous pulse coupling, and can readily be analyzed with respect to emergent collective behavior.

For instantaneous synaptic interactions, I have proved that collective oscillations can emerge only when the recurrent input includes a voltage component. This is the case, for example, for electrical coupling via gap junctions. In the absence of gap junctions, the recurrent synaptic input can incorporate a voltage component—and hence allows for collective

oscillations—if pulses transmitted via chemical synapses have a finite width or if the pulse peaks at a moment different from the neuron's spike time. This insight strongly supports the voltage-dependent spike synchronization mechanism (Devalle et al., 2017), a resonance in the neurons' membrane and spiking dynamics (Pyle & Rosenbaum, 2017), that is crucial for collective oscillations and typically not captured by traditional firing rate models.

Symmetric pulses centered about the spike time support collective oscillations in principle, but the parameter region where collective oscillations can be found appears somewhat degenerate due to the close vicinity of a Hopf bifurcation curve—where oscillations emerge supercritically—and a homoclinic bifurcation curve—at which oscillations are destroyed. Relaxing the symmetry condition of the pulse, or shifting the pulse peak away from the spike time, generates a wide region in parameter space where collective oscillations arise naturally and as the unique attractor of the network dynamics. I have shown in networks of inhibitory QIF neurons with excitatory drive ($J < 0, I_0 > 0$) that shifting the bulk of the pulse only slightly to the phase after the actual spike yielded robust ING oscillations. Moreover, the collective dynamics generated by instantaneous asymmetric pulses resembled those generated by first-order synapses with δ-spikes (Devalle et al., 2017). In general, however, the correspondence between pulses of finite width and more detailed models of synaptic transmission is elusive. Put differently, (narrow) pulse-coupling complements, but does not replace, synaptic kinetics and conductance-based synapses.

As an outlook and to bring the presented formalism even closer to experimental data, I leave for future work the analysis of pulse-triggered synaptic kinetics or conductance-based synapses (see the augmented RV dynamics, equation 5.10 or 5.11) or when incorporating finite threshold and reset values and asymmetric spikes with $v_p \neq -v_r$ as considered by Montbrió and Pazó (2020) and Gast et al. (2023; see also appendix H). I mention in passing that one can also transform the QIF dynamics around realistic resting potentials ≈ -70 mV (see appendix C) without changing the overall collective dynamics qualitatively. In the work presented in this article, I did not consider habituation or activity-dependent modulation of synaptic transmission, which allowed me to disentangle the effect of the pulse shape on the collective dynamics. To do so, I introduced voltage-dependent pulses in section 2.3 that arise through the interplay of a synaptic activation function with the action potential and thus directly account for its shape. The shape of the action potential, that is, its waveform, is not only cell type and temperature dependent (Sabatini & Regehr, 1999; Gray & McCormick, 1996; Bean, 2007), but may also undergo dynamic changes through various plasticity mechanisms (Sabatini & Regehr, 1999; Bean, 2007; Byrne & Kandel, 1996). These can lead to action potential broadening or amplitude reduction, which subsequently affects neurotransmitter release and synaptic transmission and may hence directly, or indirectly, contribute

to learning and memory storage (Gershman, 2023). The proposed pulse coupling is versatile to incorporate dynamical changes of the action potential, which will open up new avenues for investigating network effects of (pre-)synaptic, intrinsic, and homeostatic plasticity complementary to previously proposed mean-field approaches (Tsodyks et al., 1998; Zierenberg et al., 2018; Schmutz et al., 2020; Pietras et al., 2022; Taher et al., 2020; Gast et al., 2020, 2021; Bandyopadhyay et al., 2022; Chen & Campbell, 2022; Taher et al., 2022; Ferrara et al., 2023; Gast et al., 2023), and leverage more detailed network simulations as in Lavi et al. (2015) that combine the computational advantages of spiking neural networks with biological realism at the microscopic level, including a more realistic synaptic transmission process.

Acknowledgments

I thank A. Pikovsky, E. Montbrió, R. Cestnik, and A. Daffertshofer for fruitful discussions. The project has received funding from the European Union's Horizon 2020 research and innovation program under the Marie Skłodowska-Curie grant agreement 101032806.

References

Abbott, L. F., & van Vreeswijk, C. (1993). Asynchronous states in networks of pulse-coupled oscillators. *Phys. Rev. E*, *48*(2), 1483. 10.1103/PhysRevE.48.1483

Afifurrahman, Ullner, E., & Politi, A. (2021). Collective dynamics in the presence of finite-width pulses. *Chaos*, *31*(4), 043135. 10.1063/5.0046691

Aguiar, M. A., Dias, A., & Field, M. (2019). Feedforward networks: Adaptation, feedback, and synchrony. *J. Nonl. Sci.*, *29*(3), 1129–1164. 10.1007/s00332-018-9513-7

Ariaratnam, J. T., & Strogatz, S. H. (2001). Phase diagram for the Winfree model of coupled nonlinear oscillators. *Phys. Rev. Lett.*, *86*(19), 4278. 10.1103/PhysRevLett.86.4278

Arkhipov, A., Gouwens, N. W., Billeh, Y. N., Gratiy, S., Iyer, R., Wei, Z., . . . Koch, C. (2018). Visual physiology of the layer 4 cortical circuit in silico. *PLOS Comput. Biol.*, *14*(11), 1–47. 10.1371/journal.pcbi.1006535

Ashwin, P., Bick, C., & Poignard, C. (2021). Dead zones and phase reduction of coupled oscillators. *Chaos*, *31*(9), 093132. 10.1063/5.0063423

Avitabile, D., Desroches, M., & Ermentrout, G. B. (2022). Cross-scale excitability in networks of quadratic integrate-and-fire neurons. *PLOS Comput. Biol.*, *18*(10), e1010569. 10.1371/journal.pcbi.1010569

Bandyopadhyay, A., Rabuffo, G., Calabrese, C., Gudibanda, K., Depannemaecker, D., Ivanov, A., . . . Petkoski, S. (2022). *Mean-field approximation of network of biophysical neurons driven by conductance-based ion exchange*. bioRxiv.

Bean, B. P. (2007). The action potential in mammalian central neurons. *Nat. Rev. Neurosci.*, *8*(6), 451–465. 10.1038/nrn2148

Bekkers, J. M., & Stevens, C. F. (1996). Cable properties of cultured hippocampal neurons determined from sucrose-evoked miniature EPSCs. *J. Neurophys.*, *75*(3), 1250–1255. 10.1152/jn.1996.75.3.1250

Bi, H., Segneri, M., di Volo, M., & Torcini, A. (2020). Coexistence of fast and slow gamma oscillations in one population of inhibitory spiking neurons. *Phys. Rev. Research*, *2*(1), 013042.

Bick, C., Goodfellow, M., Laing, C. R., & Martens, E. A. (2020). Understanding the dynamics of biological and neural oscillator networks through exact mean-field reductions: A review. *J. Math. Neurosci.*, *10*(1), 9. 10.1186/s13408-020-00086-9

Billeh, Y. N., Cai, B., Gratiy, S. L., Dai, K., Iyer, R., Gouwens, N. W., . . . Arkhipov, A. (2020). Systematic integration of structural and functional data into multi-scale models of mouse primary visual cortex. *Neuron*, *106*(3), 388–403. 10.1016/j.neuron.2020.01.040

Bîrdac, L., Kaslik, E., & Mureş, R. (2022). Dynamics of a reduced system connected to the investigation of an infinite network of identical theta neurons. *Mathematics*, *10*(18), 3245.

Bläsche, C., Means, S., & Laing, C. R. (2020). Degree assortativity in networks of spiking neurons. *J. Comput. Dyn.*, *7*(2), 401–423.

Börgers, C. (2017). *An introduction to modeling neuronal dynamics*. Springer.

Börgers, C., & Kopell, N. (2003). Synchronization in networks of excitatory and inhibitory neurons with sparse, random connectivity. *Neural Comput.*, *15*(3), 509–538.

Börgers, C., & Kopell, N. (2005). Effects of noisy drive on rhythms in networks of excitatory and inhibitory neurons. *Neural Comput.*, *17*(3), 557–608.

Brunel, N., & Hakim, V. (1999). Fast global oscillations in networks of integrate-and-fire neurons with low firing rates. *Neural Comput.*, *11*(7), 1621–1671. 10.1162/089976699300016179

Brunel, N., & Hansel, D. (2006). How noise affects the synchronization properties of recurrent networks of inhibitory neurons. *Neural Comput.*, *18*(5), 1066–1110. 10.1162/neco.2006.18.5.1066

Brunel, N., & Wang, X.-J. (2003). What determines the frequency of fast network oscillations with irregular neural discharges? I. Synaptic dynamics and excitation-inhibition balance. *J. Neurophysiol.*, *90*(1), 415–430. 10.1152/jn.01095.2002

Burkitt, A. N. (2006). A review of the integrate-and-fire neuron model: I. Homogeneous synaptic input. *Biol. Cybern.*, *95*(1), 1–19. 10.1007/s00422-006-0068-6

Byrne, Á., Brookes, M. J., & Coombes, S. (2017). A mean field model for movement induced changes in the beta rhythm. *J. Comput. Neurosci.*, *43*, 143–158. 10.1007/s10827-017-0655-7

Byrne, A., O'Dea, R. D., Forrester, M., Ross, J., & Coombes, S. (2020). Next-generation neural mass and field modeling. *J. Neurophys.*, *123*(2), 726–742. 10.1152/jn.00406.2019

Byrne, Á., Ross, J., Nicks, R., & Coombes, S. (2022). Mean-field models for EEG/MEG: From oscillations to waves. *Brain Topography*, *35*(1), 36–53. 10.1007/s10548-021-00842-4

Byrne, J. H., & Kandel, E. R. (1996). Presynaptic facilitation revisited: State and time dependence. *J. Neurosci.*, *16*(2), 425–435. 10.1523/JNEUROSCI.16-02-00425.1996

Catllá, A. J., Schaeffer, D. G., Witelski, T. P., Monson, E. E., & Lin, A. L. (2008). On spiking models for synaptic activity and impulsive differential equations. *SIAM Review*, *50*(3), 553–569.

Catterall, W. A. (2011). Voltage-gated calcium channels. *Cold Spring Harb. Perspect Biol.*, *3*(8), a003947. 10.1101/cshperspect.a003947

Cestnik, R., & Pikovsky, A. (2022a). Hierarchy of exact low-dimensional reductions for populations of coupled oscillators. *Phys. Rev. Lett.*, *128*(5), 054101. 10.1103/PhysRevLett.128.054101

Cestnik, R., & Pikovsky, A. (2022b). Exact finite-dimensional reduction for a population of noisy oscillators and its link to Ott–Antonsen and Watanabe–Strogatz theories. *Chaos*, *32*(11), 113126. 10.1063/5.0106171

Chandra, S., Hathcock, D., Crain, K., Antonsen, T. M., Girvan, M., & Ott, E. (2017). Modeling the network dynamics of pulse-coupled neurons. *Chaos*, *27*(3), 033102. 10.1063/1.4977514

Chao, O. Y., & Yang, Y.-M. (2019). Timing constraints of action potential evoked CA2+ current and transmitter release at a central nerve terminal. *Sci. Rep.*, *9*(1), 1–14. 10.1038/s41598-018-37186-2

Chen, L., & Campbell, S. A. (2022). Exact mean-field models for spiking neural networks with adaptation. *J. Comp. Neurosci.*, *50*(4), 445–469. 10.1007/s10827-022-00825-9

Clusella, P., Köksal-Ersöz, E., Garcia-Ojalvo, J., & Ruffini, G. (2022). Comparison between an exact and a heuristic neural mass model with second-order synapses. *Biol. Cybern.*, *117*(1–2), 1–15. 10.1007/s00422-022-00952-7

Clusella, P., & Montbrió, E. (2022). *Regular and sparse neuronal synchronization are described by identical mean field dynamics*. arXiv:2208.05515.

Clusella, P., Pietras, B., & Montbrió, E. (2022). Kuramoto model for populations of quadratic integrate-and-fire neurons with chemical and electrical coupling. *Chaos*, *32*(1), 013105. 10.1063/5.0075285

Contessa, P., & Luca, C. J. D. (2013). Neural control of muscle force: Indications from a simulation model. *J. Neurophys.*, *109*(6), 1548–1570. 10.1152/jn.00237.2012

Coombes, S., & Byrne, Á. (2019). *Next generation neural mass models*. Springer.

Daido, H. (1996). Onset of cooperative entrainment in limit-cycle oscillators with uniform all-to-all interactions: Bifurcation of the order function. *Physica D*, *91*(1–2), 24–66. 10.1016/0167-2789(95)00260-X

Destexhe, A., Mainen, Z. F., & Sejnowski, T. J. (1994). Synthesis of models for excitable membranes, synaptic transmission and neuromodulation using a common kinetic formalism. *J. Comput. Neurosci.*, *1*(3), 195–230. 10.1007/BF00961734

Devalle, F., Montbrió, E., & Pazó, D. (2018). Dynamics of a large system of spiking neurons with synaptic delay. *Phys. Rev. E*, *98*(4), 042214. 10.1103/PhysRevE.98.042214

Devalle, F., Roxin, A., & Montbrió, E. (2017). Firing rate equations require a spike synchrony mechanism to correctly describe fast oscillations in inhibitory networks. *PLOS Comput. Biol.*, *13*(12), e1005881. 10.1371/journal.pcbi.1005881

di Volo, M., Segneri, M., Goldobin, D. S., Politi, A., & Torcini, A. (2022). Coherent oscillations in balanced neural networks driven by endogenous fluctuations. *Chaos*, *32*(2), 023120. 10.1063/5.0075751

di Volo, M., & Torcini, A. (2018). Transition from asynchronous to oscillatory dynamics in balanced spiking networks with instantaneous synapses. *Phys. Rev. Lett.*, *121*(12), 128301. 10.1103/PhysRevLett.121.128301

Doedel, E. J., Champneys, A. R., Dercole, F., Fairgrieve, T. F., Kuznetsov, Y. A., Oldeman, B., . . . Zhang, C. (2007). *AUTO-07P: Continuation and bifurcation software for ordinary differential equations*. Concordia University technical report.

Dumont, G., & Gutkin, B. (2019). Macroscopic phase resetting-curves determine oscillatory coherence and signal transfer in inter-coupled neural circuits. *PLOS Comput. Biol.*, *15*(5), e1007019. 10.1371/journal.pcbi.1007019

Ermentrout, G. B. (1996). Type I membranes, phase resetting curves, and synchrony. *Neural Comput.*, *8*(5), 979–1001. 10.1162/neco.1996.8.5.979

Ermentrout, G. B. (2006). Gap junctions destroy persistent states in excitatory networks. *Phys. Rev. E*, *74*, 031918. 10.1103/PhysRevE.74.031918

Ermentrout, G. B., & Kopell, N. (1986). Parabolic bursting in an excitable system coupled with a slow oscillation. *SIAM J. Appl. Math.*, *46*(2), 233–253. 10.1137/0146017

Ermentrout, G. B., & Kopell, N. (1990). Oscillator death in systems of coupled neural oscillators. *SIAM J. Appl. Math.*, *50*(1), 125–146. 10.1137/0150009

Ermentrout, G. B., & Kopell, N. (1998). Fine structure of neural spiking and synchronization in the presence of conduction delays. *Proc. Nat. Acad. Sci.*, *95*(3), 1259–1264. 10.1073/pnas.95.3.1259

Ermentrout, G. B., & Terman, D. H. (2010). *Mathematical foundations of neuroscience*. Springer.

Feketa, P., Klinshov, V., & Lücken, L. (2021). A survey on the modeling of hybrid behaviors: How to account for impulsive jumps properly. *Comm. Nonl. Sci. Num. Sim.*, *103*, 105955.

Ferrara, A., Angulo-Garcia, D., Torcini, A., & Olmi, S. (2023). Population spiking and bursting in next-generation neural masses with spike-frequency adaptation. *Phys. Rev. E*, *107*, 024311. 10.1103/PhysRevE.107.024311

Fuglevand, A. J., Winter, D. A., & Patla, A. E. (1993). Models of recruitment and rate coding organization in motor-unit pools. *J. Neurophys.*, *70*(6), 2470–2488. 10.1152/jn.1993.70.6.2470

Gallego, R., Montbrió, E., & Pazó, D. (2017). Synchronization scenarios in the Winfree model of coupled oscillators. *Phys. Rev. E*, *96*, 042208. 10.1103/PhysRevE.96.042208

Gast, R., Knösche, T. R., & Schmidt, H. (2021). Mean-field approximations of networks of spiking neurons with short-term synaptic plasticity. *Phys. Rev. E*, *104*, 044310. 10.1103/PhysRevE.104.044310

Gast, R., Rose, D., Salomon, C., Möller, H. E., Weiskopf, N., & Knösche, T. R. (2019). PyRates—a Python framework for rate-based neural simulations. *PLOS One*, *14*(12), e0225900. 10.1371/journal.pone.0225900

Gast, R., Schmidt, H., & Knösche, T. R. (2020). A mean-field description of bursting dynamics in spiking neural networks with short-term adaptation. *Neural Comput.*, *32*(9), 1615–1634. 10.1162/neco_a_01300

Gast, R., Solla, S. A., & Kennedy, A. (2023). Macroscopic dynamics of neural networks with heterogeneous spiking thresholds. *Phys. Rev. E*, *107*, 024306. 10.1103/PhysRevE.107.024306

Gershman, S. J. (2023). The molecular memory code and synaptic plasticity: A synthesis. *Biosystems*, *224*, 104825. 10.1016/j.biosystems.2022.104825

Gerstner, W., & Kistler, W. M. (2002). *Spiking neuron models: Single neurons, populations, plasticity*. Cambridge University Press.

Goel, P., & Ermentrout, G. B. (2002). Synchrony, stability, and firing patterns in pulse-coupled oscillators. *Physica D*, *163*(3–4), 191–216. 10.1016/S0167-2789(01)00374-8

Golomb, D., Wang, X.-J., & Rinzel, J. (1996). Propagation of spindle waves in a thalamic slice model. *J. Neurophys.*, *75*(2), 750–769. 10.1152/jn.1996.75.2.750

Gray, C. M., & McCormick, D. A. (1996). Chattering cells: Superficial pyramidal neurons contributing to the generation of synchronous oscillations in the visual cortex. *Science*, *274*(5284), 109–113. 10.1126/science.274.5284.109

Gutkin, B. S. (2014). *Theta-neuron model*. Springer.

Gutkin, B. S., & Ermentrout, G. B. (1998). Dynamics of membrane excitability determine interspike interval variability: A link between spike generation mechanisms and cortical spike train statistics. *Neural Comput.*, *10*(5), 1047–1065. 10.1162/089976698300017331

Gutkin, B. S., Laing, C. R., Colby, C., Chow, C. C., & Ermentrout, G. B. (2001). Turning on and off with excitation: The role of spike-timing asynchrony and synchrony in sustained neural activity. *J. Comput. Neurosci.*, *11*(2), 121–134. 10.1023/A:1012837415096

Hansel, D., & Mato, G. (2001). Existence and stability of persistent states in large neuronal networks. *Phys. Rev. Lett.*, *86*(18), 4175.

Hansel, D., & Mato, G. (2003). Asynchronous states and the emergence of synchrony in large networks of interacting excitatory and inhibitory neurons. *Neural Comput.*, *15*(1), 1–56. 10.1162/089976603321043685

Hoppensteadt, F. C., & Izhikevich, E. M. (1997). *Weakly connected neural networks*. Springer.

Humphries, M. (2021). *The spike: An epic journey through the brain in 2.1 seconds*. Princeton University Press.

Izhikevich, E. M. (1999). Class 1 neural excitability, conventional synapses, weakly connected networks, and mathematical foundations of pulse-coupled models. *IEEE Trans. Neural Netw.*, *10*(3), 499–507. 10.1109/72.761707

Izhikevich, E. M. (2007). *Dynamical systems in neuroscience: The geometry of excitability and bursting*. MIT Press.

Jüttner, B., Henriksen, C., & Martens, E. A. (2021). Birth and destruction of collective oscillations in a network of two populations of coupled type 1 neurons. *Chaos*, *31*(2), 023141.

Kaeser, P. S., & Regehr, W. G. (2014). Molecular mechanisms for synchronous, asynchronous, and spontaneous neurotransmitter release. *Ann. Rev. Physiol.*, *76*, 333. 10.1146/annurev-physiol-021113-170338

Kato, S., & Jones, M. C. (2015). A tractable and interpretable four-parameter family of unimodal distributions on the circle. *Biometrika*, *102*(1), 181–190. 10.1093/biomet/asu059

Keeley, S., Byrne, A., Fenton, A., & Rinzel, J. (2019). Firing rate models for gamma oscillations. *Journal of Neurophysiology*, *121*(6), 2181–2190. 10.1152/jn.00741.2018

Klinshov, V., Lücken, L., & Feketa, P. (2021). On the interpretation of Dirac pulses in differential equations for phase oscillators. *Chaos*, *31*(3), 031102.

Koch, C. (2004). *Biophysics of computation: Information processing in single neurons*. Oxford University Press.

Kömek, K., Ermentrout, G. B., Walker, C. P., and Cho, R. Y. (2012). Dopamine and gamma band synchrony in schizophrenia. Insights from computational and empirical studies. *Eur. J. Neurosci.*, *36*(2), 2146–2155.

Kopell, N., Ermentrout, G. B., Whittington, M. A., & Traub, R. D. (2000). Gamma rhythms and beta rhythms have different synchronization properties. *Proc. Nat. Acad. Sci.*, *97*(4), 1867–1872. 10.1073/pnas.97.4.1867

Kotani, K., Yamaguchi, I., Yoshida, L., Jimbo, Y., & Ermentrout, G. B. (2014). Population dynamics of the modified theta model: Macroscopic phase reduction and bifurcation analysis link microscopic neuronal interactions to macroscopic gamma oscillation. *J. R. Soc. Interface*, *11*(95), 20140058. 10.1098/rsif.2014.0058

Kuramoto, Y. (1984). *Chemical oscillations, waves and turbulence*. Springer.

Kuramoto, Y., Shinomoto, S., & Sakaguchi, H. (1987). *Active rotator model for large populations of oscillatory and excitable elements*. Springer.

Kuznetsov, Y. A. (1998). *Elements of applied bifurcation theory*. Springer.

Laing, C. R. (2014). Derivation of a neural field model from a network of theta neurons. *Phys. Rev. E*, *90*, 010901(R). 10.1103/PhysRevE.90.010901

Laing, C. R. (2015). Exact neural fields incorporating gap junctions. *SIAM J. Appl. Dyn. Syst.*, *14*(4), 1899–1929. 10.1137/15M1011287

Laing, C. R. (2016a). Bumps in small-world networks. *Front. Comput. Neurosci.*, *10*, 53. 10.3389/fncom.2016.00053

Laing, C. R. (2016b). Travelling waves in arrays of delay-coupled phase oscillators. *Chaos*, *26*(9), 094802. 10.1063/1.4953663

Laing, C. R. (2017). *Phase oscillator network models of brain dynamics*. Wiley.

Laing, C. R. (2018a). The dynamics of networks of identical theta neurons. *J. Math. Neurosci.*, *8*(1), 1–24. 10.1186/s13408-018-0059-7

Laing, C. R. (2018b). Chaos in small networks of theta neurons. *Chaos*, *28*(7), 073101. 10.1063/1.5028515

Laing, C. R., & Bläsche, C. (2020). The effects of within-neuron degree correlations in networks of spiking neurons. *Biol. Cybern.*, *114*(3), 337–347. 10.1007/s00422-020-00822-0

Laing, C. R., & Omel'chenko, O. (2020). Moving bumps in theta neuron networks. *Chaos*, *30*(4), 043117. 10.1063/1.5143261

Latham, P. E., Richmond, B., Nelson, P., & Nirenberg, S. (2000). Intrinsic dynamics in neuronal networks. I. Theory. *J. Neurophysiol.*, *83*(2), 808–827. 10.1152/jn.2000.83.2.808

Lavi, A., Perez, O., & Ashery, U. (2015). Shaping neuronal network activity by presynaptic mechanisms. *PLOS Comput. Biol.*, *11*(9), e1004438. 10.1371/journal.pcbi.1004438

Lin, L., Barreto, E., & So, P. (2020). Synaptic diversity suppresses complex collective behavior in networks of theta neurons. *Front. Comput. Neurosci.*, *14*, 44. 10.3389/fncom.2020.00044

Luke, T. B., Barreto, E., & So, P. (2013). Complete classification of the macroscopic behavior of a heterogeneous network of theta neurons. *Neural Comput.*, *25*, 3207–3234.

Luke, T. B., Barreto, E., & So, P. (2014). Macroscopic complexity from an autonomous network of networks of theta neurons. *Front. Comput. Neurosci.*, *8*, 145. 10.3389/fncom.2014.00145

Maex, R., & De Schutter, E. (2003). Resonant synchronization in heterogeneous networks of inhibitory neurons. *J. Neurosci.*, *23*(33), 10503–10514. 10.1523/JNEUROSCI.23-33-10503.2003

Means, S. A., Bläsche, C., & Laing, C. R. (2020). A permutation method for network assembly. *PLOS One*, *15*(10), e0240888. 10.1371/journal.pone.0240888

Mensi, S., Naud, R., Pozzorini, C., Avermann, M., Petersen, C. C., & Gerstner, W. (2012). Parameter extraction and classification of three cortical neuron types reveals two distinct adaptation mechanisms. *J. Neurophys.*, *107*(6), 1756–1775. 10.1152/jn.00408.2011

Montbrió, E., & Pazó, D. (2020). Exact mean-field theory explains the dual role of electrical synapses in collective synchronization. *Phys. Rev. Lett.*, *125*(24), 248101.

Montbrió, E., Pazó, D., & Roxin, A. (2015). Macroscopic description for networks of spiking neurons. *Phys. Rev. X*, *5*(2), 021028.

O'Keeffe, K. P., & Strogatz, S. H. (2016). Dynamics of a population of oscillatory and excitable elements. *Phys. Rev. E*, *93*, 062203.

Omel'chenko, O., & Laing, C. R. (2022). Collective states in a ring network of theta neurons. *Proc. R. Soc. A*, *478*(2259), 20210817.

Osan, R., & Ermentrout, G. B. (2001). Two dimensional synaptically generated traveling waves in a theta-neuron neural network. *Neurocomputing*, *38*, 789–795. 10.1016/S0925-2312(01)00390-3

Ott, E., & Antonsen, T. M. (2008). Low dimensional behavior of large systems of globally coupled oscillators. *Chaos*, *18*(3), 037113.

Pazó, D., & Montbrió, E. (2014). Low-dimensional dynamics of populations of pulse-coupled oscillators. *Phys. Rev. X*, *4*(1), 011009.

Pazó, D., & Montbrió, E. (2016). From quasiperiodic partial synchronization to collective chaos in populations of inhibitory neurons with delay. *Phys. Rev. Lett.*, *116*(23), 238101.

Pfeiffer, P., Gowers, R., Schleimer, J., & Schreiber, S. (2023). Large-scale analysis of diversity of neuronal excitability types in the Allen Brain Cell database. Poster presented at the Bernstein Conference, Berlin. 10.12751/nncn.bc2023.281.

Pietras, B., Cestnik, R., & Pikovsky, A. (2023). Exact finite-dimensional description for networks of globally coupled spiking neurons. *Phys. Rev. E*, *107*, 024315. 10.1103/PhysRevE.107.024315

Pietras, B., & Daffertshofer, A. (2019). Network dynamics of coupled oscillators and phase reduction techniques. *Phys. Rep.*, *819*, 1–105. 10.1016/j.physrep.2019.06.001

Pietras, B., Devalle, F., Roxin, A., Daffertshofer, A., & Montbrió, E. (2019). Exact firing rate model reveals the differential effects of chemical versus electrical synapses in spiking networks. *Phys. Rev. E*, *100*, 042412. 10.1103/PhysRevE.100.042412

Pietras, B., Schmutz, V., & Schwalger, T. (2022). Mesoscopic description of hippocampal replay and metastability in spiking neural networks with short-term plasticity. *PLOS Comput. Biol.*, *18*(12), 1–46. 10.1371/journal.pcbi.1010809

Pozzorini, C., Mensi, S., Hagens, O., Naud, R., Koch, C., & Gerstner, W. (2015). Automated high-throughput characterization of single neurons by means of simplified spiking models. *PLOS Comput. Biol.*, *11*(6), e1004275. 10.1371/journal.pcbi.1004275

Pyle, R., & Rosenbaum, R. (2017). Spatiotemporal dynamics and reliable computations in recurrent spiking neural networks. *Phys. Rev. Lett.*, *118*(1), 018103. 10.1103/PhysRevLett.118.018103

Raikova, R. T., & Aladjov, H. T. (2002). Hierarchical genetic algorithm versus static optimization: Investigation of elbow flexion and extension movements. *J. Biomech.*, *35*(8), 1123–1135. 10.1016/S0021-9290(02)00031-3

Ratas, I., & Pyragas, K. (2016). Macroscopic self-oscillations and aging transition in a network of synaptically coupled quadratic integrate-and-fire neurons. *Phys. Rev. E*, *94*(3), 032215. 10.1103/PhysRevE.94.032215

Ratas, I., & Pyragas, K. (2018). Macroscopic oscillations of a quadratic integrate- and-fire neuron network with global distributed-delay coupling. *Phys. Rev. E*, *98*(5), 052224. 10.1103/PhysRevE.98.052224

Ratas, I., & Pyragas, K. (2019). Noise-induced macroscopic oscillations in a network of synaptically coupled quadratic integrate-and-fire neurons. *Phys. Rev. E*, *100*(5), 052211. 10.1103/PhysRevE.100.052211

Rössert, C., Pozzorini, C., Chindemi, G., Davison, A. P., Eroe, C., King, J., . . . Muller, E. (2017). Automated point-neuron simplification of data-driven microcircuit models.

Rothman, J. S. (2013). *Modeling synapses*. Springer.

Rotstein, H. G. (2015). Subthreshold amplitude and phase resonance in models of quadratic type: Nonlinear effects generated by the interplay of resonant and amplifying currents. *J. Comp. Neurosci.*, *38*(2), 325–354. 10.1007/s10827-014-0544-2

Roulet, J., & Mindlin, G. B. (2016). Average activity of excitatory and inhibitory neural populations. *Chaos*, *26*(9), 093104. 10.1063/1.4962326

Roxin, A., Brunel, N., & Hansel, D. (2005). Role of delays in shaping spatiotemporal dynamics of neuronal activity in large networks. *Phys. Rev. Lett.*, *94*(23), 238103. 10.1103/PhysRevLett.94.238103

Roxin, A., & Montbrió, E. (2011). How effective delays shape oscillatory dynamics in neuronal networks. *Physica D*, *240*(3), 323–345. 10.1016/j.physd.2010.09.009

Sabatini, B. L., & Regehr, W. G. (1996). Timing of neurotransmission at fast synapses in the mammalian brain. *Nature*, *384*(6605), 170–172. 10.1038/384170a0

Sabatini, B., & Regehr, W. (1999). Timing of synaptic transmission. *Annu. Rev. Physiol.*, *61*(1), 521–542. 10.1146/annurev.physiol.61.1.521

Sato, Y. D., & Shiino, M. (2007). Generalization of coupled spiking models and effects of the width of an action potential on synchronization phenomena. *Phys. Rev. E*, *75*(1), 011909.

Schmutz, V., Gerstner, W., & Schwalger, T. (2020). Mesoscopic population equations for spiking neural networks with synaptic short-term plasticity. *J. Math. Neurosci.*, *10*(1), 1–32. 10.1186/s13408-020-00082-z

Shinomoto, S., & Kuramoto, Y. (1986). Phase transitions in active rotator systems. *Progress of Theoretical Physics*, *75*(5), 1105–1110. 10.1143/PTP.75.1105

Skinner, F. K., Kopell, N., & Marder, E. (1994). Mechanisms for oscillation and frequency control in reciprocally inhibitory model neural networks. *J. Comput. Neurosci.*, *1*(1), 69–87. 10.1007/BF00962719

Smeal, R. M., Ermentrout, G. B., & White, J. A. (2010). Phase-response curves and synchronized neural networks. *Philos. Transactions Royal Soc. B: Biol. Sci.*, *365*, 2407–2422. 10.1098/rstb.2009.0292

So, P., Luke, T. B., & Barreto, E. (2014). Networks of theta neurons with time-varying excitability: Macroscopic chaos, multistability, and final-state uncertainty. *Physica D*, *267*, 16–26. 10.1016/j.physd.2013.04.009

Taher, H., Avitabile, D., & Desroches, M. (2022). Bursting in a next generation neural mass model with synaptic dynamics: A slow–fast approach. *Nonlinear Dyn.*, *108*(4), 4261–4285. 10.1007/s11071-022-07406-6

Taher, H., Torcini, A., & Olmi, S. (2020). Exact neural mass model for synaptic-based working memory. *PLOS Comput. Biol.*, *16*(12), 1–42. 10.1371/journal.pcbi.1008533

Teeter, C., Iyer, R., Menon, V., Gouwens, N., Feng, D., Berg, J., . . . Mihalas, S. (2018). Generalized leaky integrate-and-fire models classify multiple neuron types. *Nature Comm.*, *9*(1), 1–15. 10.1038/s41467-017-02717-4

Treves, A. (1993). Mean-field analysis of neuronal spike dynamics. *Network*, *4*(3), 259.

Tsodyks, M., Pawelzik, K., & Markram, H. (1998). Neural networks with dynamic synapses. *Neural Comput.*, *10*(4), 821–835. 10.1162/089976698300017502

Turnquist, A. G. R., & Rotstein, H. G. (2018). *Quadratization: From conductance-based models to caricature models with parabolic nonlinearities*. Springer.

Van Hook, M. J. (2020). Temperature effects on synaptic transmission and neuronal function in the visual thalamus. *PLOS One*, *15*(4), e0232451. 10.1371/journal.pone.0232451

Van Vreeswijk, C., Abbott, L. F., & Ermentrout, G. B. (1994). When inhibition not excitation synchronizes neural firing. *J. Comput. Neurosci.*, *1*(4), 313–321. 10.1007/BF00961879

Volgushev, M., Kudryashov, I., Chistiakova, M., Mukovski, M., Niesmann, J., & Eysel, U. T. (2004). Probability of transmitter release at neocortical synapses at different temperatures. *J. Neurophys.*, *92*(1), 212–220. 10.1152/jn.01166.2003

Wang, B., & Dudko, O. K. (2021). A theory of synaptic transmission. *eLife*, *10*, e73585.

Wang, X.-J. (2010). Neurophysiological and computational principles of cortical rhythms in cognition. *Physiol. Rev.*, *90*(3), 1195–1268. 10.1152/physrev.00035.2008

Wang, X.-J., & Buzsáki, G. (1996). Gamma oscillation by synaptic inhibition in a hippocampal interneuronal network model. *J. Neurosci.*, *16*(20), 6402–6413. 10.1523/JNEUROSCI.16-20-06402.1996

Wang, X.-J., & Rinzel, J. (1992). Alternating and synchronous rhythms in reciprocally inhibitory model neurons. *Neural Comput.*, *4*(1), 84–97. 10.1162/neco.1992.4.1.84

White, J. A., Chow, C. C., Rit, J., Soto-Trevinõ, C., & Kopell, N. (1998). Synchronization and oscillatory dynamics in heterogeneous, mutually inhibited neurons. *J. Comput. Neurosci.*, *5*(1), 5–16. 10.1023/A:1008841325921

Wilson, H. R. (1999). *Spikes, decisions, and actions: The dynamical foundations of neuroscience*. Oxford University Press.

Wilson, H. R., & Cowan, J. D. (1972). Excitatory and inhibitory interactions in localized populations of model neurons. *Biophys. J.*, *12*(1), 1–24. 10.1016/S0006-3495(72)86068-5

Winfree, A. T. (1967). Biological rhythms and the behavior of populations of coupled oscillators. *J. Theor. Biol.*, *16*(1), 15–42. 10.1016/0022-5193(67)90051-3

Winfree, A. T. (1980). *The geometry of biological time*. Springer.

Yang, Y.-M., & Wang, L.-Y. (2006). Amplitude and kinetics of action potential-evoked CA2+ current and its efficacy in triggering transmitter release at the developing calyx of held synapse. *J. Neurosci.*, *26*(21), 5698–5708. 10.1523/JNEUROSCI.4889-05.2006

Zierenberg, J., Wilting, J., & Priesemann, V. (2018). Homeostatic plasticity and external input shape neural network dynamics. *Phys. Rev. X*, *8*, 031018.

Zillmer, R., Livi, R., Politi, A., & Torcini, A. (2007). Stability of the splay state in pulse-coupled networks. *Phys. Rev. E*, *76*(4), 046102. 10.1103/PhysRevE.76.046102

Received May 5, 2023; accepted March 18, 2024.